Three-body $D\bar{D}\pi$ dynamics for the $X(3872)$

V. Baru and A. A. Filin

Institut für Theoretische Physik II, Ruhr-Universität Bochum, D-44780 Bochum,

Germany and Institute for Theoretical and Experimental Physics,

B. Cheremushkinskaya 25, 117218 Moscow, Russia

C. Hanhart

Forschungszentrum Jülich, Institute for Advanced Simulation,

Institut für Kernphysik (Theorie) and Jülich Center

for Hadron Physics, D-52425 Jülich, Germany

Yu. S. Kalashnikova, A. E. Kudryavtsev, and A. V. Nefediev

Institute for Theoretical and Experimental Physics,

B. Cheremushkinskaya 25, 117218 Moscow, Russia

We investigate the role played by the three-body $D\bar{D}\pi$ dynamics on the near-threshold resonance $X(3872)$ charmonium state, which is assumed to be formed by nonperturbative $D\bar{D}^*$ dynamics. It is demonstrated that, as compared to the naive static-pions approximation, the imaginary parts that originate from the inclusion of dynamical pions reduce substantially the width from the $D\bar{D}\pi$ intermediate state. In particular, for a resonance peaked at 0.5 MeV below the $D^0\bar{D}^{*0}$ threshold, this contribution to the width is reduced by about a factor of 2, and the effect of the pion dynamics on the width grows as long as the resonance is shifted towards the $D^0\bar{D}^0\pi^0$ threshold. Although the physical width of the X is dominated by inelastic channels, our finding should still be of importance for the X line shapes in the $D\bar{D}\pi$ channel below $D\bar{D}^*$ threshold. For example, in the scattering length approximation, the imaginary part of the scattering length includes effects of all the pion dynamics and does not only stem from the D^* width. Meanwhile, we find that another important quantity for the X phenomenology, the residue at the X pole, is weakly sensitive to dynamical pions. In particular, we find that the binding energy dependence of this quantity from the full calculation is close to that found from a model with pointlike $D\bar{D}^*$ interactions only, consistent with earlier claims. Coupled-channel

effects (inclusion of the charged $D\bar{D}^*$ channel) turn out to have a moderate impact on the results.

I.   INTRODUCTION

Over the past decade we have witnessed fascinating progress in charmonium spectroscopy, especially, due to the development of B-factories, the mass region above the open-charm threshold became accessible for a systematic, high-statistics experimental investigation. As a result, many new and unexpected states (the so-called "X, Y, Z states") with unusual properties were discovered—for a recent review see Ref. [1]. Among these new charmonium-like states the $X(3872)$ meson found by Belle Collaboration in 2003 [2] is the best-studied state both experimentally and theoretically. However, the $X(3872)$ still remains enigmatic, and there is no consensus on the nature of this state.

The proximity of the X to the $D^0\bar{D}^{*0}$ threshold suggests the dynamical (molecular) interpretation, though other options like $c\bar{c}$ or tetraquark charmonium are discussed as well. The $X(3872)$ was observed both in the $J/\psi\pi^+\pi^-$ ($J/\psi\rho$) and $J/\psi\pi^+\pi^-\pi^0$ ($J/\psi\omega$) modes [3, 4], which points to isospin violation in the wave function of the X. It is readily explained in the molecular picture as due to the large (about 8 MeV) mass difference between the charged and neutral $D\bar{D}^*$ thresholds: the isospin violation is enhanced due to kinematical reasons, as the effective phase space available in the case of the ρ is much larger than that in the case of the ω [5, 6]. A molecular interpretation implies the 1^{++} quantum numbers for the $X(3872)$ and, until recently, this assignment was commonly accepted and supported by observation of the X in the $D^0\bar{D}^{*0}$ decay mode [7–9]. However, while the analysis of the $J/\psi\pi^+\pi^-$ decay mode of the $X(3872)$ yields either 1^{++} or 2^{-+} quantum numbers [3], the recent analysis of the $J/\psi\pi^+\pi^-\pi^0$ mode seems to favour the 2^{-+} assignment [4], though the 1^{++} option is not excluded. As shown in Ref. [10], the X cannot be a naive $c\bar{c}$ 2^{-+} state and, were the 2^{-+} quantum numbers confirmed, very exotic explanations for the X would have to be invoked. In the absence of such a confirmation we stick to the most conventional 1^{++} assignment for the X.

Threshold affinity should lead to a significant admixture of the pertinent charmed meson pair in the wave function of the resonance, whatever the nature of the $X(3872)$ is, though it cannot *per se* shed any light on the origin of binding mechanisms responsible for the

formation of the X. A natural explanation for the $X(3872)$ would be a $c\bar{c}\ 2^3P_1$ charmonium state (χ'_{c1}), residing at the $D^0\bar{D}^{*0}$ threshold, but, unless the coupling of the quark state to the charmed mesons channel is unnaturally small, the naive bare $c\bar{c}$ spectrum should be distorted strongly by coupled-channel effects. Indeed, the microscopic calculations [11, 12] confirm this pattern: the $X(3872)$ pole can be generated dynamically by a strong coupling of the bare χ'_{c1} state to the $D\bar{D}^*$ hadronic channel, with a large admixture of the $D\bar{D}^*$ component, see also Ref. [13] where the fine-tuning of the χ'_{c1} state to the $D\bar{D}^*$ threshold was discussed based on the analysis of line shapes for the $X(3872)$.

A competing approach is a traditional one-pion exchange (OPE) one. Historically, long before the charmonium revolution of 2003, pion exchange between charmed mesons was considered as a mechanism able to bind the isosinglet $D\bar{D}^*$ mesonic system and to form a deuteronlike state near threshold—see, for example, Refs. [14, 15]. Immediately after discovery of the $X(3872)$, the OPE model was revisited [16, 17]. For the most recent work on the possibility for the OPE to bind the $D\bar{D}^*$ system see Refs. [18, 19]. Further implications of the nearby pion threshold are discussed in Refs. [20, 21]. In Refs. [18, 19] divergent integrals are made finite through the introduction of suitable form factors, and bound states are found in the static approximation for the pion and neglecting the imaginary parts of the potential. Only the neutral $D^0\bar{D}^{*0}$ configuration was studied in Ref. [18], and the dependence of the binding energy on the form factor cut off parameter Λ was investigated. It was shown that the bound state in the $D^0\bar{D}^{*0}$ system, with the binding energy around 1 MeV, exists only for the values of Λ of order of 6 GeV, that is for the values much larger than admitted by interpretation of the form factors in terms of quark models. The charged $D\bar{D}^*$ channel was included in Ref. [19], and it was argued there that even for small cut offs of order of $1-2$ GeV, a bound state with a binding energy of 1 MeV appears. This result is interpreted then as a proof that the OPE provides enough attraction to produce a bound state. Notice, however, that the $D^*D\pi$ coupling constant employed in calculations of Ref. [19] is too large, and is not compatible with the data on the $D^*D\pi$ decays.

The above-mentioned calculations treated the $D\bar{D}^*$ system in a deuteronlike fashion: pions enter there in the form of a static potential. There is, however, an important difference between the deuteron and the X: the D^{*0} mass is very close to the $D^0\pi^0$ threshold. A natural worry [5] is that in the $D\bar{D}^*$ system, bound by the OPE, the pion may go on shell. The latter calls for the proper inclusion of the three-body $D\bar{D}\pi$ unitarity cuts. As shown in

Ref. [22], the cut effects are of paramount importance in the charmed $D_\alpha \bar{D}_\beta$ system if one of the constituents has a large width, dominated by the S-wave $D_\beta \to D_\alpha \pi$ decay: bound states found in Ref. [23] in the static approximation disappear completely from the spectrum if the full three-body treatment is invoked. In the case of the $X(3872)$ the generic two-body $D\pi$ interaction goes via the D^* and is in a P-wave. Due to this "P-wave penalty" one should not expect disastrous consequences, though cut effects could distort strongly the resonance shape. Indeed, inclusion of the D^* finite width alone is known to produce a spectacular bound-state peak in the $D^0 \bar{D}^0 \pi^0$ mass distribution—see Refs. [24–27]. This justifies a full investigation of the role played by the three-body dynamics on a near-threshold resonance, which is the subject of the present paper.

One of the most important findings of our study is that the X-dynamics, and especially the value of the effective coupling constant $X \to D\bar{D}^*$, is, in the molecular scenario, completely fixed by the X binding energy E_B, as long as $E_B \ll \Delta M$, with $\Delta M = 8.08$ MeV being the distance to the next (charged) two-body threshold, in line with the properties of a true two-body state, although there are various thresholds near by. This is in line with the results of Ref. [28], where the interplay of scales was studied for the case of the presence of S-wave interactions only. At the same time, by an explicit calculation, we have shown the validity of the central assumption underlying the X-EFT [21, 29], namely, that pion effects can be treated perturbatively for most observables. At leading order in such an EFT, pions can be integrated out and predictions for the observables can be made based on universal asymptotic behaviour of the $D\bar{D}^*$ wave function [30].

The most striking effect of dynamical pions is seen in their effect on the imaginary parts from the $D\bar{D}\pi$ intermediate states. Specifically, the part of the X width stemming from the width of the D^* gets cut in half once dynamical pions are included. A similar effect is observed once the three-body $D\bar{D}\pi$ cut is accounted in the $D\bar{D}^*$ potential: the imaginary part of the $D\bar{D}^*$ potential gets reduced by a factor of more than 2 compared to that for the static pion potential which leads to a further reduction of the X width. In total the width of the X from the $D\bar{D}\pi$ intermediate states is reduced from 102 to 44 keV due to the effects of dynamical pions. This observation could be of relevance for the X line shapes below the elastic threshold.

The paper is organised as follows. In Secs. II A and B we introduce the notations and derive the system of dynamical Faddeev-type equations for the $D\bar{D}^*$ scattering. In
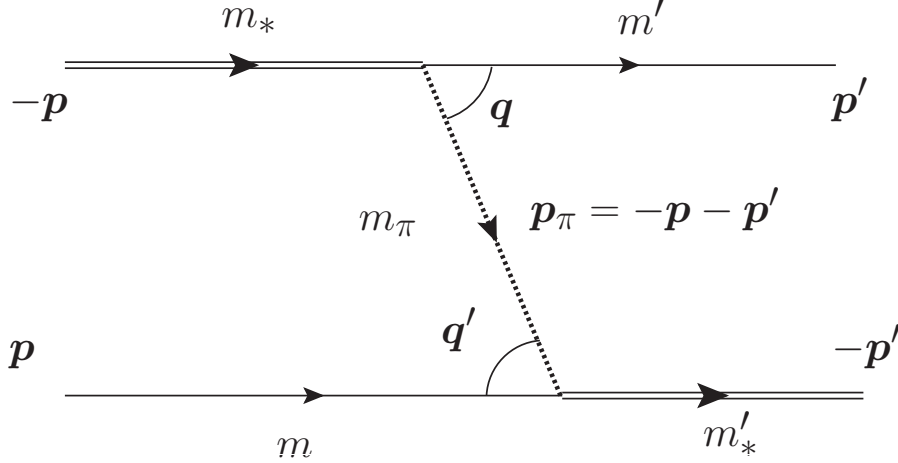
FIG. 1: Kinematics of the $D\bar{D}^*$ scattering due to the OPE. Double lines denote D^*'s while single lines denote D's.

Sec. II C we apply these equations to the $X(3872)$ assuming 1^{++} assignment for this state. Physical implications are discussed in Sec. III. First, we compare the residues of the $D\bar{D}^*$ scattering amplitude calculated with purely contact $D\bar{D}^*$ potential (with no pions) to our full dynamical results. We also discuss the role of coupled-channel dynamics for the residue. Then, assuming that the $X(3872)$ has a resonance state with the peak at $E_B = 0.5$ MeV below the $D^0\bar{D}^{*0}$ threshold, we calculate the $D^0\bar{D}^0\pi^0$ line shape within our fully dynamical treatment and compare it with various approximations. The summary of the most important results is given in Sec. IV.

II.   THREE-BODY FORMALISM

A.   Kinematics and main definitions

Consider first three channels:

$$|2\rangle = D\bar{D}^*, \quad |\bar{2}\rangle = \bar{D}D^*, \quad |3\rangle = D\bar{D}\pi, \tag{1}$$

coupled by the OPE—see Fig. 1 with $m' = m$ and $m'_* = m_*$ since, for a time being, we ignore isospins; the isospin structure of the interaction will be considered in detail below. Here m and m_* are the mass of the $D(\bar{D})$ and the bare mass of the $D^*(\bar{D}^*)$, respectively.

The dynamical equations that emerge are basically a diagrammatic representation of those presented in Ref. [31]. In the centre-of-mass frame the momenta in the two-body systems $D\bar{D}^*$ and $\bar{D}D^*$ are defined as

$$\boldsymbol{p}_D = \boldsymbol{p}, \quad \boldsymbol{p}_{\bar{D}^*} = -\boldsymbol{p}, \qquad (2)$$

$$\boldsymbol{p}_{\bar{D}} = \bar{\boldsymbol{p}}, \quad \boldsymbol{p}_{D^*} = -\bar{\boldsymbol{p}}, \qquad (3)$$

while, in the three-body $D\bar{D}\pi$ system, the momenta can be defined in terms of two sets of Jacobi variables, $\{\boldsymbol{p}, \boldsymbol{q}\}$ and $\{\bar{\boldsymbol{p}}, \bar{\boldsymbol{q}}\}$:

$$\boldsymbol{p}_D = \boldsymbol{p}, \quad \boldsymbol{p}_{\bar{D}} = -\boldsymbol{q} - \frac{m}{m + m_\pi}\boldsymbol{p}, \quad \boldsymbol{p}_\pi = \boldsymbol{q} - \frac{m_\pi}{m + m_\pi}\boldsymbol{p}, \qquad (4)$$

or

$$\boldsymbol{p}_D = -\bar{\boldsymbol{q}} - \frac{m}{m + m_\pi}\bar{\boldsymbol{p}}, \quad \boldsymbol{p}_{\bar{D}} = \bar{\boldsymbol{p}}, \quad \boldsymbol{p}_\pi = \bar{\boldsymbol{q}} - \frac{m_\pi}{m + m_\pi}\bar{\boldsymbol{p}}. \qquad (5)$$

Jacobi variables belonging to different sets are related to each other as

$$\bar{\boldsymbol{q}} = \alpha\boldsymbol{q} + \beta\boldsymbol{p}, \quad \bar{\boldsymbol{p}} = -\boldsymbol{q} - \alpha\boldsymbol{p}, \qquad (6)$$

$$\boldsymbol{q} = \alpha\bar{\boldsymbol{q}} + \beta\bar{\boldsymbol{p}}, \quad \boldsymbol{p} = -\bar{\boldsymbol{q}} - \alpha\bar{\boldsymbol{p}}, \qquad (7)$$

where

$$\alpha = \frac{m}{m + m_\pi}, \quad \beta = \alpha^2 - 1 = -\frac{(2m + m_\pi)m_\pi}{(m + m_\pi)^2}.$$

The $D\bar{D}^*\pi$ vertex is

$$v_{D\bar{D}^*\pi}(\boldsymbol{q}) = g\,\boldsymbol{\epsilon}\cdot\boldsymbol{q}, \qquad (8)$$

where $\boldsymbol{\epsilon}$ is the D^* polarisation vector, $\boldsymbol{q}$ is the relative momentum in the $D\pi$ system, and g is the coupling constant—in general here one could also introduce a form factor, however, since we are interested in near-threshold phenomena, such a form factor would not change the general properties of the results. The constant g can be fixed from the $D^{*0} \to D^0\pi^0$ width via

$$\Gamma(D^{*0} \to D^0\pi^0) \equiv \Gamma_* = \frac{8\pi^2}{3}g^2\mu_q(D^0\pi^0)\left[2\mu_q(D^0\pi^0)(m_{0*} - m_0 - m_{\pi^0})\right]^{3/2}, \qquad (9)$$

where the reduced mass is defined as

$$\mu_q(XY) = \frac{m_X m_Y}{m_X + m_Y}. \qquad (10)$$

Then the channels (1) communicate via the interaction potentials

$$V_{32}^m(\boldsymbol{p}, \boldsymbol{q}; \boldsymbol{p}') = gq_m\delta(\boldsymbol{p} - \boldsymbol{p}'), \tag{11}$$

$$V_{3\bar{2}}^m(\bar{\boldsymbol{p}}, \bar{\boldsymbol{q}}; \bar{\boldsymbol{p}}') = g\bar{q}_m\delta(\bar{\boldsymbol{p}} - \bar{\boldsymbol{p}}'), \tag{12}$$

and similarly for V_{23}^m and $V_{\bar{2}3}^m$.

The inverse two- and three-body free propagators are defined by

$$D_2(\boldsymbol{p}) = m + m_* + \frac{p^2}{2\mu_*} - M, \quad D_3(\boldsymbol{p}, \boldsymbol{q}) = 2m + m_\pi + \frac{p^2}{2\mu_p} + \frac{q^2}{2\mu_q} - M, \tag{13}$$

with M being the mass of the system, which can be expressed, for example, in terms of the energy related to the $D\bar{D}^*$ threshold, while the reduced masses are defined as

$$\mu_* = \frac{mm_*}{m + m_*}, \quad \mu_p = \frac{m(m + m_\pi)}{2m + m_\pi}, \quad \mu_q \equiv \mu_q(D\pi) = \frac{mm_\pi}{m + m_\pi}, \tag{14}$$

and, nonrelativistically, $\mu_* = \mu_p$.

Finally, we define the bare $D\pi$ self-energy $\Sigma(p)$ as

$$\Sigma(p) = \frac{g^2}{3} \int \frac{q^2 d^3q}{D_3(\boldsymbol{p}, \boldsymbol{q})}. \tag{15}$$

B.   Three–body equation for the t matrix: One-pion exchange potential

The dynamical equation for the t matrix $t_{ik}^{mn}(\boldsymbol{p}, \boldsymbol{p}')$, where $i, k = 2, \bar{2}, 3$ and m and n are the Lorentz indices, reads schematically:

$$t = V - V\mathcal{G}_0 t, \tag{16}$$

where $\mathcal{G}_0$ is the diagonal matrix of the free Green's functions (13) and the interaction potential V possesses just two nontrivial components given by Eqs. (11) and (12). The system of nine equations (16) splits into three decoupled subsystems:

$$\begin{cases} t_{22} = -V_{23}\dfrac{1}{D_3}t_{32} \\[2mm] t_{\bar{2}2} = -V_{\bar{2}3}\dfrac{1}{D_3}t_{32} \\[2mm] t_{32} = V_{32} - V_{32}\dfrac{1}{D_2}t_{22} - V_{3\bar{2}}\dfrac{1}{D_2}t_{\bar{2}2}, \end{cases} \tag{17}$$

$$\begin{cases} t_{2\bar{2}} = -V_{23}\dfrac{1}{D_3}t_{3\bar{2}} \\[2mm] t_{\bar{2}\bar{2}} = -V_{\bar{2}3}\dfrac{1}{D_3}t_{3\bar{2}} \\[2mm] t_{3\bar{2}} = V_{3\bar{2}} - V_{32}\dfrac{1}{D_2}t_{2\bar{2}} - V_{3\bar{2}}\dfrac{1}{D_2}t_{\bar{2}\bar{2}}, \end{cases} \tag{18}$$

$$
\begin{cases}
t_{23} = V_{23} - V_{23}\dfrac{1}{D_3}t_{33} \\[2mm]
t_{\bar{2}3} = V_{\bar{2}3} - V_{\bar{2}3}\dfrac{1}{D_3}t_{33} \\[2mm]
t_{33} = -V_{32}\dfrac{1}{D_2}t_{23} - V_{3\bar{2}}\dfrac{1}{D_2}t_{\bar{2}3}.
\end{cases}
\tag{19}
$$

Below, in this chapter, we give schematically the derivation of the three-body equations for the t matrix which follows from Eqs. (17)-(19). To simplify notations distinguish neither between $V_{\bar{2}3}$ and V_{23} nor between $V_{3\bar{2}}$ and V_{32}. We also omit all arguments. The full and detailed derivation can be found in the Appendix.

In the systems (17) and (18) we exclude the third equation and, using the definition (15), arrive at

$$
\begin{cases}
t_{22} = -\Sigma + \Sigma\dfrac{1}{D_2}t_{22} + V_{23}\dfrac{1}{D_3}V_{32}\dfrac{1}{D_2}t_{\bar{2}2} \\[2mm]
t_{\bar{2}2} = -V_{\bar{2}3}\dfrac{1}{D_3}V_{32} + \Sigma\dfrac{1}{D_2}t_{\bar{2}2} + V_{\bar{2}3}\dfrac{1}{D_3}V_{32}\dfrac{1}{D_2}t_{22},
\end{cases}
\tag{20}
$$

and a similar system for the components $t_{2\bar{2}}$ and $t_{\bar{2}\bar{2}}$, which we do not quote here. Note that the relations between the breakup amplitudes t_{23} and $t_{\bar{2}3}$ and the two-body amplitudes $t_{2\bar{2}}$ and $t_{\bar{2}\bar{2}}$ are given in Appendix A.

The interaction respects C parity, so it is possible to define C-even and C-odd $D\bar{D}^*$ matrix elements. Indeed, the system (20) can be rewritten for the combinations

$$
t_\pm = t_{22} \pm t_{\bar{2}2},
\tag{21}
$$

which satisfy then the following equations:

$$
\Delta\frac{1}{D_2}t_\pm = -\Sigma \mp V_{23}\frac{1}{D_3}V_{32} \pm V_{23}\frac{1}{D_3}V_{32}\frac{1}{D_2}t_\pm,
\tag{22}
$$

where the inverse dressed D^* propagator $\Delta(p)$ is introduced as

$$
\Delta(p) = m_* + m + \frac{p^2}{2\mu_*} - M - \Sigma(p).
\tag{23}
$$

Finally, substituting

$$
t_\pm = -\frac{\Sigma D_2}{\Delta} + \frac{D_2}{\Delta}a_\pm\frac{D_2}{\Delta},
\tag{24}
$$

one arrives at the following equation for the new function $a_\pm^{mn}(\boldsymbol{p},\boldsymbol{p}')$:

$$
a_\pm = V_\pm - V_\pm\Delta^{-1}a_\pm,
\tag{25}
$$

which, in the full form (see the Appendix), reads

$$
a_\pm^{mn}(\boldsymbol{p},\boldsymbol{p}',E) = V_\pm^{mn}(\boldsymbol{p},\boldsymbol{p}') - \int d^3s\, V_\pm^{mp}(\boldsymbol{p},\boldsymbol{s})\Delta^{-1}(s)a_\pm^{pn}(\boldsymbol{s},\boldsymbol{p}',E),
\tag{26}
$$

where the generic OPE potential has the form:

$$V_\pm^{mn}(\boldsymbol{p}, \boldsymbol{p}') = \mp g^2 \frac{(\boldsymbol{p}' + \alpha\boldsymbol{p})_m (\boldsymbol{p} + \alpha\boldsymbol{p}')_n}{D_3(\boldsymbol{p}, \boldsymbol{p}')}, \quad \alpha = \frac{m}{m_\pi + m}. \tag{27}$$

In what follows we confine ourselves to the C-even states only and therefore we consider only the amplitude $a_+^{mn}(\boldsymbol{p}, \boldsymbol{p}') \equiv a^{mn}(\boldsymbol{p}, \boldsymbol{p}')$ and the corresponding potential $V_+^{mn}(\boldsymbol{p}, \boldsymbol{p}') \equiv V^{mn}(\boldsymbol{p}, \boldsymbol{p}')$.

Equation (26) was derived neglecting isospin. However, in the case of the $X(3872)$, the two two-body thresholds, the neutral $D^0\bar{D}^{*0} +$ c.c. threshold and the charged one $D^+D^{*-} +$ c.c., are split by only around 8 MeV, so they are both potentially relevant, and Eq. (26) is to be modified accordingly.

For antimesons, we stick to the convention of Ref. [19], that is we define

$$|\bar{M}\rangle = \hat{C}|M\rangle, \tag{28}$$

where $\hat{C}$ is the C-parity transformation operator, and $|M\rangle$ ($|\bar{M}\rangle$) denotes the wave function of the meson (antimeson). Then interpolating currents of the pions and the D and D^* meson involved are chosen as

$$\pi^0 = \frac{1}{\sqrt{2}}(\bar{u}\gamma_5 u - \bar{d}\gamma_5 d), \quad \pi^+ = \bar{d}\gamma_5 u, \quad \pi^- = \bar{u}\gamma_5 d, \tag{29}$$

$$D^0 = \bar{u}\gamma_5 c, \quad \bar{D}^0 = \bar{c}\gamma_5 u, \quad D^+ = \bar{d}\gamma_5 c, \quad D^- = \bar{c}\gamma_5 d, \tag{30}$$

$$D^{*0} = \bar{u}\gamma_\mu c, \quad \bar{D}^{*0} = -\bar{c}\gamma_\mu u, \quad D^{*+} = \bar{d}\gamma_\mu c, \quad D^{*-} = -\bar{c}\gamma_\mu d. \tag{31}$$

Since the pion is an isovector, the isospin structure of the OPE potential (27) is given by the product $\vec{\tau}_1 \cdot \vec{\tau}_2$. Therefore, in order to evaluate the isospin coefficients, we are to compute the matrix element $\langle i|\vec{\tau}_1 \cdot \vec{\tau}_2|k\rangle$ for $i, k = 0, \bar{0}, c$, and $\bar{c}$, where the latter states are defined as:

$$|0\rangle = D^0\bar{D}^{*0}, \quad |\bar{0}\rangle = \bar{D}^0 D^{*0}, \quad |c\rangle = D^+D^{*-}, \quad |\bar{c}\rangle = D^- D^{*+}. \tag{32}$$

This will define the full OPE potentials $V_{ik}^{mn}(\boldsymbol{p}, \boldsymbol{p}')$. Notice that, since strong interactions respect C-parity, then the following relation holds:

$$\langle i|\vec{\tau}_1 \cdot \vec{\tau}_2|\bar{k}\rangle = \langle \bar{i}|\vec{\tau}_1 \cdot \vec{\tau}_2|k\rangle, \quad i, k = 0, c. \tag{33}$$

It is easy to find then for the two nonvanishing coefficients:

$$\langle 0|\vec{\tau}_1 \cdot \vec{\tau}_2|\bar{0}\rangle = \langle c|\vec{\tau}_1 \cdot \vec{\tau}_2|\bar{c}\rangle = 1 \quad \text{(neutral pion exchange)},$$
$$\langle 0|\vec{\tau}_1 \cdot \vec{\tau}_2|\bar{c}\rangle = \langle c|\vec{\tau}_1 \cdot \vec{\tau}_2|\bar{0}\rangle = 2 \quad \text{(charged pion exchange)}. \tag{34}$$

It is clear therefore that nonvanishing OPE potentials are (see Fig. 1):

$$V_{00}^{mn}(\boldsymbol{p}, \boldsymbol{p}') = V_{\overline{00}}^{mn}(\boldsymbol{p}, \boldsymbol{p}'), \text{ with } m = m' = m_0, \ m_\pi = m_{\pi^0}, \tag{35}$$

$$V_{c\bar{c}}^{mn}(\boldsymbol{p}, \boldsymbol{p}') = V_{\bar{c}c}^{mn}(\boldsymbol{p}, \boldsymbol{p}'), \text{ with } m = m' = m_c, \ m_\pi = m_{\pi^0}, \tag{36}$$

$$V_{c\bar{0}}^{mn}(\boldsymbol{p}, \boldsymbol{p}') = V_{\bar{c}0}^{mn}(\boldsymbol{p}, \boldsymbol{p}'), \text{ with } m = m_0, \ m' = m_c, \ m_\pi = m_{\pi^c}, \tag{37}$$

$$V_{0\bar{c}}^{mn}(\boldsymbol{p}, \boldsymbol{p}') = V_{\bar{0}c}^{mn}(\boldsymbol{p}, \boldsymbol{p}'), \text{ with } m = m_c, \ m' = m_0, \ m_\pi = m_{\pi^c}, \tag{38}$$

where m_0, m_c, m_{π^0}, and m_{π^c} are the masses of the neutral and charged D meson, and the pions, respectively. The factor of 2 needed for charge-exchange potentials [see Eq. (34)] will be introduced in the scattering equations explicitly.

The explicit form of the OPE potentials can be obtained then as the generalisation of the generic potential (27):

$$V_{ik}^{mn}(\boldsymbol{p}, \boldsymbol{p}') = (\boldsymbol{p}' + \alpha_{ik}\boldsymbol{p})^m (\boldsymbol{p} + \alpha'_{ik}\boldsymbol{p}')^n F_{ik}(\boldsymbol{p}, \boldsymbol{p}'), \quad F_{ik}(\boldsymbol{p}, \boldsymbol{p}') = -\frac{g^2}{D_{3ik}(\boldsymbol{p}, \boldsymbol{p}')}, \tag{39}$$

with

$$\alpha_{00} = \alpha'_{00} = \frac{m_0}{m_{\pi^0} + m_0}, \quad \alpha_{cc} = \alpha'_{cc} = \frac{m_c}{m_{\pi^0} + m_c},$$
$$\alpha_{0c} = \alpha'_{c0} = \frac{m_c}{m_{\pi^c} + m_c}, \quad \alpha_{c0} = \alpha'_{0c} = \frac{m_0}{m_{\pi^c} + m_0},$$

and

$$D_{300}(\boldsymbol{p}, \boldsymbol{p}') = 2m_0 + m_{\pi^0} + \frac{p^2}{2m_0} + \frac{p'^2}{2m_0} + \frac{(\boldsymbol{p} + \boldsymbol{p}')^2}{2m_{\pi^0}} - M - i0,$$
$$D_{3cc}(\boldsymbol{p}, \boldsymbol{p}') = 2m_c + m_{\pi^0} + \frac{p^2}{2m_c} + \frac{p'^2}{2m_c} + \frac{(\boldsymbol{p} + \boldsymbol{p}')^2}{2m_{\pi^0}} - M - i0,$$
$$D_{30c}(\boldsymbol{p}, \boldsymbol{p}') = m_c + m_0 + m_{\pi^c} + \frac{p^2}{2m_0} + \frac{p'^2}{2m_c} + \frac{(\boldsymbol{p} + \boldsymbol{p}')^2}{2m_{\pi^c}} - M - i0,$$
$$D_{3c0}(\boldsymbol{p}, \boldsymbol{p}') = m_c + m_0 + m_{\pi^c} + \frac{p^2}{2m_c} + \frac{p'^2}{2m_0} + \frac{(\boldsymbol{p} + \boldsymbol{p}')^2}{2m_{\pi^c}} - M - i0. \tag{40}$$

The 16-component OPE interaction potential $V_{ik}^{mn}(\boldsymbol{p}, \boldsymbol{p}')$ gives rise to a system of coupled equations for the 16 components of the $D\bar{D}^*$ scattering t matrix. However, due to symmetries of the OPE potential (35)–(38), many t matrix components coincide with one another. In particular, it is easy to demonstrate that

$$a_{ik}^{mn} = a_{\bar{i}\bar{k}}^{mn}, \quad a_{\bar{i}k}^{mn} = a_{i\bar{k}}^{mn}, \quad i, k = 0, c, \tag{41}$$

so that only eight independent t matrix components remain and split into two groups, four components in each, which satisfy two disentangled subsystems of equations. In what

follows we shall be interested in the $|0\rangle$ final state, so we consider only the first subsystem of equations of these two, which reads

$$
\begin{cases}
a_{00}^{mn}(\boldsymbol{p},\boldsymbol{p}',E) = V_{00}^{mn}(\boldsymbol{p},\boldsymbol{p}') - \int \frac{d^3 s}{\Delta_0(s)} V_{00}^{mp}(\boldsymbol{p},\boldsymbol{s}) a_{00}^{pn}(\boldsymbol{s},\boldsymbol{p}',E) \\
\qquad\qquad\qquad\qquad - 2\int \frac{d^3 s}{\Delta_c(s)} V_{0c}^{mp}(\boldsymbol{p},\boldsymbol{s}) a_{c0}^{pn}(\boldsymbol{s},\boldsymbol{p}',E) \\
a_{c0}^{mn}(\boldsymbol{p},\boldsymbol{p}',E) = 2V_{c0}^{mn}(\boldsymbol{p},\boldsymbol{p}') - 2\int \frac{d^3 s}{\Delta_0(s)} V_{c0}^{mp}(\boldsymbol{p},\boldsymbol{s}) a_{00}^{pn}(\boldsymbol{s},\boldsymbol{p}',E) \\
\qquad\qquad\qquad\qquad - \int \frac{d^3 s}{\Delta_c(s)} V_{cc}^{mp}(\boldsymbol{p},\boldsymbol{s}) a_{c0}^{pn}(\boldsymbol{s},\boldsymbol{p}',E).
\end{cases}
\tag{42}
$$

C. 1^{++} channel

From now on we stick to the quantum numbers inherent to the $X(3872)$ charmonium, assuming the latter to be 1^{++} as per discussion in the Introduction. To perform the partial-wave decomposition of the scattering equation (42) we expand the amplitude and the potential in terms of the spherical vectors $\boldsymbol{Y}_{JLM}(\boldsymbol{n})$:

$$
a_{ik}^{mn}(\boldsymbol{p},\boldsymbol{p}',E) = \sum_{J}\sum_{L_1 L_2} a_{ik}^{J,L_1,L_2}(p,p',E) \sum_{M} (\boldsymbol{Y}_{JL_1M}(\boldsymbol{n}))^m (\boldsymbol{Y}_{JL_2M}^*(\boldsymbol{n}'))^n,
\tag{43}
$$

$$
V_{ik}^{mn}(\boldsymbol{p},\boldsymbol{p}') = \sum_{J}\sum_{L_1 L_2} V_{ik}^{J,L_1,L_2}(p,p') \sum_{M} (\boldsymbol{Y}_{JL_1M}(\boldsymbol{n}))^m (\boldsymbol{Y}_{JL_2M}^*(\boldsymbol{n}'))^n,
\tag{44}
$$

where $\boldsymbol{n}$ and $\boldsymbol{n}'$ are the unit vectors for the momenta $\boldsymbol{p}$ and $\boldsymbol{p}'$, respectively, and, given the chosen quantum numbers, the relevant matrix elements are those with $J = 1$ and $L_1, L_2 = 0, 2$. To simplify notations, we omit everywhere the superscript for the total momentum $J = 1$.

Furthermore, once we are interested only in the S-wave in final state, we need to know only the a_{ik}^{SS} and a_{ik}^{DS} matrix elements of the amplitude, so that we use the following decomposition of the amplitude:

$$
a_{ik}^{mn}(\boldsymbol{p},\boldsymbol{p}',E) = a_{ik}^{SS}(p,p',E)T_{SS}^{mn} + a_{ik}^{DS}(p,p',E)T_{DS}^{mn},
\tag{45}
$$

where, using properties of the spherical vectors, one can find for the projectors:

$$
T_{SS}^{mn} = \frac{1}{4\pi}\delta_{mn}, \quad T_{DS}^{mn} = \frac{1}{4\pi\sqrt{2}}(\delta_{mn} - 3n_m n_m)
\tag{46}
$$

and, consequently, for the four nonvanishing matrix elements of the potential:

$$
\begin{aligned}
V_{ik}^{SS}(p,p') &= \frac{2\pi}{3} \int_{-1}^{1} F_{ik}(p,p',x)\left(\alpha_{ik}p^2 + \alpha'_{ik}p'^2 + (\alpha_{ik}\alpha'_{ik}+1)pp'x\right)dx, \\
V_{ik}^{SD}(p,p') &= -\frac{2\pi\sqrt{2}}{3} \int_{-1}^{1} F_{ik}(p,p',x)\left(\alpha'_{ik}p'^2 + \alpha_{ik}p^2\left(\frac{3}{2}x^2 - \frac{1}{2}\right) + (\alpha_{ik}\alpha'_{ik}+1)pp'x\right)dx, \\
V_{ik}^{DS}(p,p') &= -\frac{2\pi\sqrt{2}}{3} \int_{-1}^{1} F_{ik}(p,p',x)\left(\alpha_{ik}p^2 + \alpha'_{ik}p'^2\left(\frac{3}{2}x^2 - \frac{1}{2}\right) + (\alpha_{ik}\alpha'_{ik}+1)pp'x\right)dx, \\
V_{ik}^{DD}(p,p') &= 2\pi \int_{-1}^{1} F_{ik}(p,p',x)\left(\frac{2}{3}(\alpha_{ik}p^2 + \alpha'_{ik}p'^2)\left(\frac{3}{2}x^2 - \frac{1}{2}\right) + \frac{10\alpha_{ik}\alpha'_{ik}+1}{15}pp'x\right. \\
&\quad + \left.\frac{3}{5}pp'\left(\frac{5}{2}x^3 - \frac{3}{2}x\right)\right)dx,
\end{aligned}
\tag{47}
$$

where $x = \cos\theta$, with θ being the angle between $\boldsymbol{p}$ and $\boldsymbol{p}'$. Then, finally, we arrive at the system of four coupled equations:

$$
\begin{aligned}
a_{00}^{SS}(p,p',E) &= V_{00}^{SS}(p,p') \\
&\quad - \int \frac{s^2 ds}{\Delta_0(s)} V_{00}^{SS}(p,s)a_{00}^{SS}(s,p',E) - \int \frac{s^2 ds}{\Delta_0(s)} V_{00}^{SD}(p,s)a_{00}^{DS}(s,p',E) \\
&\quad - 2\int \frac{s^2 ds}{\Delta_c(s)} V_{0c}^{SS}(p,s)a_{c0}^{SS}(s,p',E) - 2\int \frac{s^2 ds}{\Delta_c(s)} V_{0c}^{SD}(p,s)a_{c0}^{DS}(s,p',E) \\
a_{00}^{DS}(p,p',E) &= V_{00}^{DS}(p,p') \\
&\quad - \int \frac{s^2 ds}{\Delta_0(s)} V_{00}^{DS}(p,s)a_{00}^{SS}(s,p',E) - \int \frac{s^2 ds}{\Delta_0(s)} V_{00}^{DD}(p,s)a_{00}^{DS}(s,p',E) \\
&\quad - 2\int \frac{s^2 ds}{\Delta_c(s)} V_{0c}^{DS}(p,s)a_{c0}^{SS}(s,p',E) - 2\int \frac{s^2 ds}{\Delta_c(s)} V_{0c}^{DD}(p,s)a_{c0}^{DS}(s,p',E) \\
a_{c0}^{SS}(p,p',E) &= 2V_{c0}^{SS}(p,p') \\
&\quad - 2\int \frac{s^2 ds}{\Delta_0(s)} V_{c0}^{SS}(p,s)a_{00}^{SS}(s,p',E) - 2\int \frac{s^2 ds}{\Delta_0(s)} V_{c0}^{SD}(p,s)a_{00}^{DS}(s,p',E) \\
&\quad - \int \frac{s^2 ds}{\Delta_c(s)} V_{cc}^{SS}(p,s)a_{c0}^{SS}(s,p',E) - \int \frac{s^2 ds}{\Delta_c(s)} V_{cc}^{SD}(p,s)a_{c0}^{DS}(s,p',E) \\
a_{c0}^{DS}(p,p',E) &= 2V_{c0}^{DS}(p,p') \\
&\quad - 2\int \frac{s^2 ds}{\Delta_0(s)} V_{c0}^{DS}(p,s)a_{00}^{SS}(s,p',E) - 2\int \frac{s^2 ds}{\Delta_0(s)} V_{c0}^{DD}(p,s)a_{00}^{DS}(s,p',E) \\
&\quad - \int \frac{s^2 ds}{\Delta_c(s)} V_{cc}^{DS}(p,s)a_{c0}^{SS}(s,p',E) - \int \frac{s^2 ds}{\Delta_c(s)} V_{cc}^{DD}(p,s)a_{c0}^{DS}(s,p',E).
\end{aligned}
\tag{48}
$$

We choose to define the energy E relative to the neutral two-body threshold:

$$
M = m_{0*} + m_0 + E.
\tag{49}
$$

The full inverse propagators Δ_0 and Δ_c entering the system of equations (48) are obtained as a generalisation of Eq. (23) through the introduction of the running width $\Gamma(p)$ which

incorporates both the effect of the self-energy $\Sigma(p)$ as well as contributions from other D^* decay channels:

$$\Delta_0(p) = m_{0*} + m_0 + \frac{p^2}{2\mu_{0*}} - M - \frac{i}{2}\Gamma_0(p), \quad \Delta_c(p) = m_{c*} + m_c + \frac{p^2}{2\mu_{c*}} - M - \frac{i}{2}\Gamma_c(p), \quad (50)$$

where the reduced masses are

$$\mu_{0*} = \frac{m_0 m_{0*}}{m_0 + m_{0*}}, \quad \mu_{c*} = \frac{m_c m_{c*}}{m_c + m_{c*}}. \tag{51}$$

The running widths $\Gamma_0(p)$ and $\Gamma_c(p)$ take the form

$$\Gamma_0(p) = \Gamma(D^{*0} \to D^0\gamma) \tag{52}$$
$$+\frac{8\pi^2}{3}g^2\left\{\mu_q(D^0\pi^0)\left[2\mu_q(D^0\pi^0)\left(M - m_0 - \frac{p^2}{2\mu_{0*}} - m_0 - m_{\pi^0}\right)\right]^{3/2}\right.$$
$$\times\Theta\left(M - m_0 - \frac{p^2}{2\mu_{0*}} - m_0 - m_{\pi^0}\right)$$
$$-i\mu_q(D^0\pi^0)\left[2\mu_q(D^0\pi^0)\left(m_0 + \frac{p^2}{2\mu_{0*}} + m_0 + m_{\pi^0} - M\right)\right]^{3/2}$$
$$\times\Theta\left(m_0 + \frac{p^2}{2\mu_{0*}} + m_0 + m_{\pi^0} - M\right)$$
$$+2\mu_q(D^+\pi^-)\left[2\mu_q(D^+\pi^-)\left(M - m_0 - \frac{p^2}{2\mu_{0*}} - m_c - m_{\pi^c}\right)\right]^{3/2}$$
$$\times\Theta\left(M - m_0 - \frac{p^2}{2\mu_{0*}} - m_c - m_{\pi^c}\right)$$
$$-2i\mu_q(D^+\pi^-)\left[2\mu_q(D^+\pi^-)\left(m_0 + \frac{p^2}{2\mu_{0*}} + m_c + m_{\pi^c} - M\right)\right]^{3/2}$$
$$\times\Theta\left(m_0 + \frac{p^2}{2\mu_{0*}} + m_c + m_{\pi^c} - M\right)$$
$$\left. +2i\mu_q(D^+\pi^-)\left[2\mu_q(D^+\pi^-)(m_c + m_{\pi^c} - m_{0*})\right]^{3/2}\right\},$$

and

$$\Gamma_c(p) = \frac{8\pi^2}{3}g^2\left\{2\mu_q(D^0\pi^+)\left[2\mu_q(D^0\pi^+)\left(M - m_c - \frac{p^2}{2\mu_{c*}} - m_0 - m_{\pi^c}\right)\right]^{3/2}\right. \tag{53}$$
$$\times\Theta\left(M - m_c - \frac{p^2}{2\mu_{c*}} - m_0 - m_{\pi^c}\right)$$
$$-2i\mu_q(D^0\pi^+)\left[2\mu_q(D^0\pi^+)\left(m_c + \frac{p^2}{2\mu_{c*}} + m_0 + m_{\pi^c} - M\right)\right]^{3/2}$$
$$\times\Theta\left(m_c + \frac{p^2}{2\mu_{c*}} + m_0 + m_{\pi^c} - M\right)$$
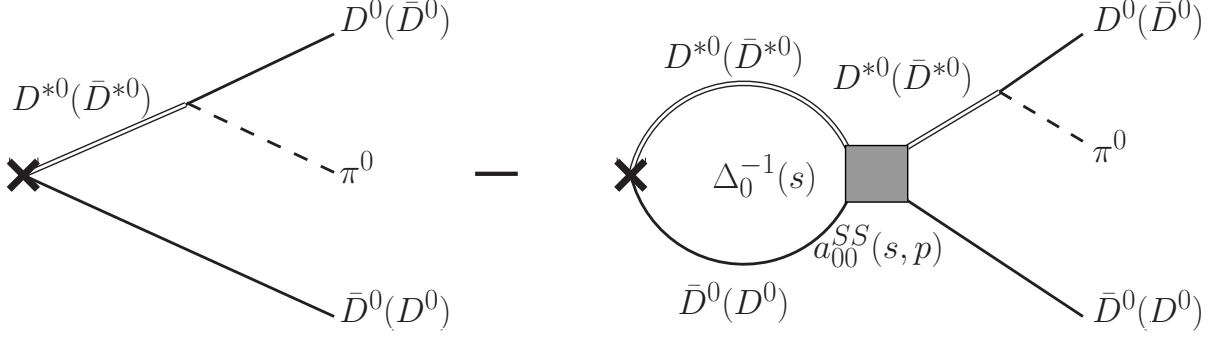
FIG. 2: The amplitude for the $D^0\bar{D}^0\pi^0$ S-wave production rate. The cross denotes the pointlike source $\mathcal{F}$.

$$+\mu_q(D^+\pi^0)\left[2\mu_q(D^+\pi^0)\left(M - m_c - \frac{p^2}{2\mu_{c*}} - m_c - m_{\pi^0}\right)\right]^{3/2}$$

$$\times\Theta\left(M - m_c - \frac{p^2}{2\mu_{c*}} - m_c - m_{\pi^0}\right)$$

$$-i\mu_q(D^+\pi^0)\left[2\mu_q(D^+\pi^0)\left(m_c + \frac{p^2}{2\mu_{c*}} + m_c + m_{\pi^0} - M\right)\right]^{3/2}$$

$$\times\Theta\left(m_c + \frac{p^2}{2\mu_{c*}} + m_c + m_{\pi^0} - M\right)\Bigg\}.$$

Note, formally there should be a radiative term also for the decay of the charged D^*, however, in this case it is negligibly small and will therefore be dropped.

The $D^0\bar{D}^0\pi^0$ S-wave rate is calculated now as (see Fig. 2)

$$\frac{dBr}{dE} = \frac{\mathcal{B}}{2\pi}\frac{m_{\pi^0}\Gamma_*}{\mu_p(2\mu_q(D^0\pi^0)E_*)^{3/2}}\int_0^{\sqrt{2\mu_p(E+E_*)}} p\,dp\int_{\bar{p}_{\min}}^{\bar{p}_{\max}}\bar{p}\,d\bar{p}$$

$$\times\Bigg\{\left(E + E_* - \frac{p^2}{2\mu_p}\right)\left|\frac{J(p,E)}{\Delta_0(p)}\right|^2 + \left(E + E_* - \frac{\bar{p}^2}{2\mu_p}\right)\left|\frac{J(\bar{p},E)}{\Delta_0(\bar{p})}\right|^2 \quad (54)$$

$$+\frac{1}{\alpha}\left[\left(\alpha^2 + 1\right)(E + E_*) - \frac{p^2 + \bar{p}^2}{2\mu_p}\right]\mathrm{Re}\left[\frac{J(p,E)}{\Delta_0(p)}\left(\frac{J(\bar{p},E)}{\Delta_0(\bar{p})}\right)^*\right]\Bigg\}$$

where

$$J(p,E) = 1 - \int_0^\infty \frac{s^2 ds}{\Delta_0(s)}a_{00}^{SS}(s,p,E),$$

$$\bar{p}_{\max,\min} = \left|\sqrt{2\mu_q(D^0\pi^0)\left(E + E_* - \frac{p^2}{2\mu_p}\right)} \pm \alpha p\right|,$$

$$E_* = m_{0*} - m_0 - m_{\pi^0}, \quad \mu_p = \frac{m_0(m_0 + m_{\pi^0})}{2m_0 + m_{\pi^0}}, \quad \alpha = \alpha_{00} = \frac{m_0}{m_{\pi^0} + m_0}.$$

The overall coefficient $\mathcal{B} = |\mathcal{F}|^2$ absorbs all the details of the short-ranged dynamics responsible for the X production. The last term in the curly brackets in Eq. (54) corresponds to the interference of the production amplitudes with the pion produced by the D^{0*} and $\bar{D}^{0*}$. In agreement with earlier claims [30], for the bound state, interference affects substantially the magnitude of the production rate below the $D^0 \bar{D}^{0*}$ threshold.

Finally, for numerical calculations, we use the following masses and widths:

$$\begin{aligned} m_0 &= m(D^0) = 1864.84 \text{ MeV}, & m_c &= m(D^\pm) = 1869.62 \text{ MeV}, \\ m_{0*} &= m(D^{*0}) = 2006.97 \text{ MeV}, & m_{c*} &= m(D^{*\pm}) = 2010.27 \text{ MeV}, \\ m_{\pi^0} &= m(\pi^0) = 134.98 \text{ MeV}, & m_{\pi^c} &= m(\pi^\pm) = 139.57 \text{ MeV}, \end{aligned} \tag{55}$$

$$\Gamma_* = \Gamma(D^{*0} \to D^0 \pi^0) = 42 \text{ keV}, \quad \Gamma(D^{*0} \to D^0 \gamma) = 21 \text{ keV}. \tag{56}$$

Then, using Eq. (9), the coupling constant g can be extracted from the $D^{*0} \to D^0 \pi^0$ width to be:

$$g = 1.29 \cdot 10^{-5} \text{ MeV}^{-3/2}. \tag{57}$$

D. Regularisation and renormalisation of the three-body equation

The system (48) is to be solved numerically. Because of the P-wave $D^* D \pi$ vertex [see Eq. (8)], the integrals on the right-hand side diverge linearly. We separate the short- and long-range dynamics of the system, where the long-range interaction is due to the OPE while the short-range one, in addition to the short-range part of the OPE, may contain other contributions, for example, due to a strong coupling of the $D\bar{D}^*$ to the quark–antiquark charmonium. This short-range dynamics is parametrised by a constant (in momentum space) $C_0(\Lambda)$ (below referred to as contact interaction or as counter term) which appears just as an extra term in the potential V_{ik}^{SS}, that is now

$$V_{ik}^{SS}(p, p') = C_0(\Lambda) + \frac{2\pi}{3} \int_{-1}^{1} F_{ik}(p, p', x) \left(\alpha_{ik} p^2 + \alpha'_{ik} p'^2 + (\alpha_{ik} \alpha'_{ik} + 1) p p' x \right) dx, \tag{58}$$

while all other components of the potential are left intact. Here Λ is the cut off parameter which regularises the integrals in Eq. (48) (we use the simplest sharp cut off prescription, that is we substitute $\int_0^\infty ds \to \int_0^\Lambda ds$). Ideally one chooses for every Λ the value of the

counter term in such a way that it neutralises the dependence of the physical observables near threshold on the cut off Λ. As we will discuss below, this does not work for some values of Λ at least for the particular regularisation used to solve the system (48). This may indicate the need of additional counter terms. However, since the residual Λ dependence is very mild in a large range of cut offs (300 MeV $\lesssim \Lambda \lesssim$ 1700 MeV and 2500 MeV $\lesssim \Lambda \lesssim$ 3800 MeV), the renormalisation with a single counter term appears to be appropriate to investigate the issues at hand—the complete discussion of the properties of the system (48) will be postponed to a subsequent publication.

III.   THE EFFECT OF DYNAMICAL PIONS ON A NEAR-THRESHOLD RESONANCE

We will now compare the solution of the full problem (48) (including the counter term discussed in the previous chapter), with the solution of the same problem in the static approximation. This implies using the static OPE potential and omitting the momentum dependence of the D^{*0} width, cf. Sec. III B and Eq. (79) for more details. In both calculations we require the system to possess a resonance at $E = -E_B$ with $E_B = 0.5$ MeV. Note that in the presence of pions there is no bound state, so we define the position of the resonance as the position of a peak in the $D^0 \bar{D}^0 \pi^0$ production rate, given by Eq. (54). Therefore, comparing the properties of the results of the two calculations we investigate the role played by dynamical pions. In addition we study the role played by the charged channel in the formation of the $X(3872)$ state.

A.   Investigation of the $D\bar{D}^*$ contact interaction

Before we proceed, we briefly discuss the calculations for a model with the contact $D\bar{D}^*$ interaction only [just retaining the C_0 term in Eq. (58)]. The advantage of this model is that it is solvable analytically and thus a comparison of this simplified model with the results of the full calculation allows one to understand better the findings. In the next subsections the corresponding equations for the single-channel as well as for the coupled-channels problem are derived, for the explicit solution will allow us to better understand some properties of the full equations.

1. Single-channel case with a contact $D\bar{D}^*$ interaction

We start from the simplest, single-channel, case of Eq. (48) with the only nonvanishing potential being $V_{00}^{SS} = C_0$. Then Eq. (48) reduces to a simple algebraic equation:

$$a_{00} = C_0 - C_0 a_{00} I_0, \tag{59}$$

where, in order to simplify notations, we set in this chapter $a_{00} \equiv a_{00}^{SS}$. Here

$$I_0(E) = \int_0^\Lambda ds \frac{s^2}{s^2/(2\mu_{0*}) - E - i0} = 2\mu_{0*}\left(\Lambda + \frac{k}{2}\left(i\pi + \log\frac{\Lambda - k}{\Lambda + k}\right)\right), \tag{60}$$

with $k^2 = 2\mu_{0*}E$.

The strength of the contact interaction C_0 is fixed by the requirement that the system possesses a bound state at $E = -E_B$ ($E_B > 0$):

$$C_0^{-1} = -I_0(-E_B), \quad a_{00}^{-1} = I_0(E) - I_0(-E_B). \tag{61}$$

To proceed we remind the reader that Eq. (59) is nothing but a toy model for the full system (48) where the cut off Λ is to be chosen large enough, that is larger than the natural scales in the full dynamical problem. This implies that $\Lambda \gg \sqrt{\mu_{0*}E_B}$ at least, so that the integral I_0 can be expanded in powers of the ratio k/Λ,

$$I_0 \approx 2\mu_{0*}\left(\Lambda + \frac{i}{2}\pi k - \frac{k^2}{\Lambda}\right) + O\left(\frac{k^4}{\Lambda^3}\right), \tag{62}$$

which corresponds to the effective-range expansion of the scattering amplitude:

$$a_{00}^{-1} = -\mu_{0*}\pi\left(-a^{-1} - ik + \frac{1}{2}r_{\rm eff}k^2\right), \tag{63}$$

where the scattering length and the effective range take the form:

$$a = \frac{1}{\sqrt{2\mu_{0*}E_B}}\frac{1}{1 - \sqrt{2\mu_{0*}E_B}\,r_{\rm eff}/2}, \quad r_{\rm eff} = \frac{4}{\pi\Lambda}. \tag{64}$$

The amplitude a_{00} possesses two poles in the complex k plane:

$$k_1 = i\sqrt{2\mu_{0*}E_B}, \quad k_2 = i\left(\frac{2}{r_{\rm eff}} - \sqrt{2\mu_{0*}E_B}\right). \tag{65}$$

In particular, for $E_B = 0.5$ MeV and $\Lambda = 500$ MeV, one finds

$$a = 6.6 \text{ fm}, \quad r_{\rm eff} = 0.5 \text{ fm}, \quad k_1 = i31.1 \text{ MeV}, \quad k_2 = i754.3 \text{ MeV}. \tag{66}$$

Finally, expanding k at the bound-state energy for $|E + E_B| \ll E_B$,

$$k = \sqrt{2\mu_{0*}E} \approx i\sqrt{2\mu_{0*}E_B}\left(1 - \frac{E + E_B}{2E_B}\right), \tag{67}$$

we arrive at the expansion of the amplitude a_{00} at the pole:

$$a_{00} = \frac{\text{Res } a_{00}}{E + E_B} \equiv \frac{g_{\text{eff}}^2}{E + E_B}, \tag{68}$$

where the residue reads

$$\text{Res } a_{00} = \frac{\kappa_0(E_B)}{\mu_{0*}^2 \pi}\left(1 - \frac{4}{\pi\Lambda}\kappa_0(E_B)\right)^{-1} = \frac{\sqrt{2\mu_{0*}E_B}}{\mu_{0*}^2\pi(1 - r_{\text{eff}}\sqrt{2\mu_{0*}E_B})}, \tag{69}$$

with $\kappa_0(E_B) = \sqrt{2\mu_{0*}E_B}$. This residue squared is shown in Fig. 3 for $\Lambda = 500$ MeV as the red (upper) dotted line. Its mild deviation from the straight line, at least for $E_B < 3$ MeV, is caused by a nonzero but small value of the effective range, so that we have, approximately,

$$g_{\text{eff}}^2 \propto \sqrt{E_B}. \tag{70}$$

Summarising, one can see that we have a large scattering length and one near-threshold pole in the k plane. The residue squared (that is g_{eff}^4) of the amplitude at the bound-state pole scales almost linearly with the bound-state energy. These results allow for a nice physical interpretation using the method suggested by S. Weinberg in the mid 60's [32]. He showed at the example of the deuteron, that an analysis of low-energy observables allowed one to quantify, in terms of the probability factor Z ($0 \leq Z \leq 1$), the admixture of the bare ("elementary") state in the wave function of a near-threshold bound state. This approach was generalised in Ref. [33] to the case when inelastic channels are present, as well as to the case of an above-threshold resonance. In particular, in Ref. [33], the connection is established between the admixture of a bare state and the structure of near-threshold singularities of the scattering amplitude. The latter was considered in Ref. [34] as a tool for resonance classification. The results of Refs. [33, 34] can be briefly summarised as follows. A state is mostly elementary, if there are two nearby poles in the scattering amplitude, which corresponds to a small scattering length, and large and negative effective range. In this case the coupling of the state to the hadronic channel is small, and the resonance line shape takes a Breit–Wigner form. The state is mostly composite, if the scattering length is large, and there is only one near-threshold pole. The effective range is of natural size (of the order of range of forces) and plays a role of a correction. This scenario requires a large coupling
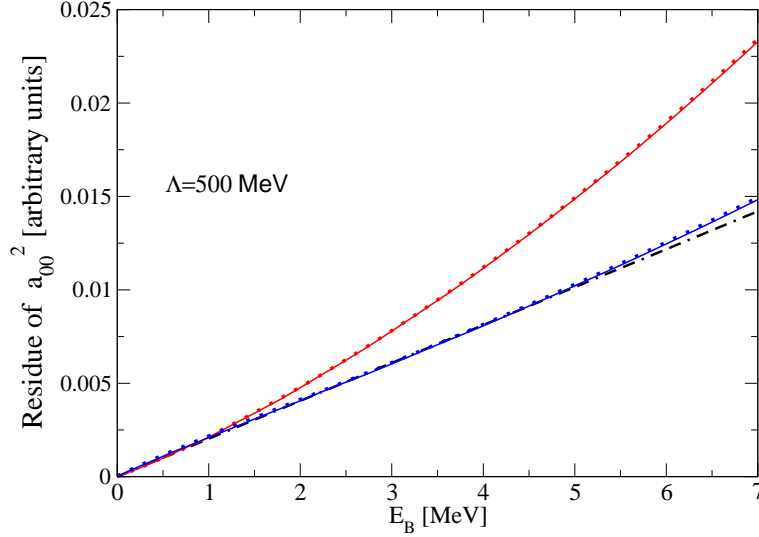
FIG. 3: Residue of the $D^0 \bar{D}^{*0}$ scattering amplitude squared versus the binding energy in the $D^0 \bar{D}^{*0}$ system. The upper, red (lower, blue) dotted curve corresponds to the solution of the single(two)-channel $D^0 \bar{D}^{*0}$ problem with the contact $D\bar{D}^*$ interaction. Solutions of the full three-body equation with dynamical pions are given by the solid lines: upper, red line—for the single-channel case and lower, blue line—for the two-channel case. The straight dot-dashed line (black) is shown to guide the eye.

of the state to the hadronic channel. In this case the wave function is dominated by its molecular component. The residue of the relevant pole is determined by the binding energy of a composite particle and thus it is model-independent. For the parameters used as an illustrative example above [see Eq. (66)] we clearly have a predominantly molecular state.

2. Two-channel case with contact $D\bar{D}^*$ interactions

In the case of two coupled channels, the scattering equation for the two components of the amplitude, for the sake of simplicity denoted in this chapter as $a_{00} \equiv a_{00}^{SS}$ and $a_{c0} \equiv a_{c0}^{SS}$, takes the form:

$$\begin{cases} a_{00} = C_0 - C_0 a_{00} I_0 - 2 C_0 a_{c0} I_c \\ a_{c0} = 2 C_0 - 2 C_0 a_{00} I_0 - C_0 a_{c0} I_c, \end{cases} \tag{71}$$

with the solution for a_{00} given by

$$a_{00} = \frac{C_0 (1 - 3 C_0 I_c)}{(1 + C_0 I_0)(1 + C_0 I_c) - 4 C_0^2 I_0 I_c}. \tag{72}$$

Similarly to the single-channel case, the integrals are

$$I_0 = \int_0^{\Lambda} ds \frac{s^2}{s^2/(2\mu_{0*}) - E - i0} \approx 2\mu_{0*}\left(\Lambda + \frac{i}{2}\pi k_0 - \frac{k_0^2}{\Lambda}\right) + O\left(\frac{k_0^4}{\Lambda^3}\right), \tag{73}$$

$$I_c = \int_0^{\Lambda} ds \frac{s^2}{s^2/(2\mu_{c*}) + \Delta M - E - i0} \approx 2\mu_{c*}\left(\Lambda + \frac{i}{2}\pi k_c - \frac{k_c^2}{\Lambda}\right) + O\left(\frac{k_c^4}{\Lambda^3}\right), \tag{74}$$

where $k_0^2 = 2\mu_{0*}E$, $k_c^2 = 2\mu_{c*}(E - \Delta M)$, and $\Delta M = m_c^* + m_c - m_0^* - m_0 = 8.08$ MeV. As before, we require that there is a bound state at $E = -E_B$, that is the amplitude (72) has a pole at this point. This leads to the equation to determine the strength of the contact term C_0. Notice that now, in the two-channel case, this equation is quadratic, as opposed to the linear equation in the single-channel case:

$$\left(1 + C_0 I_0(-E_B)\right)\left(1 + C_0 I_c(-E_B)\right) - 4C_0^2 I_0(-E_B)I_c(-E_B) = 0. \tag{75}$$

It is easy to verify that the latter equation always possesses two opposite-sign solutions for the C_0. In particular, for $\Lambda = 500$ MeV and $E_B = 0.5$ MeV these solutions are $C_0 = 13.442 \times 10^{-7}$ MeV^{-2} and $C_0 = -4.425 \times 10^{-7}$ MeV^{-2}.

Notice that the coupled-channel problem is still dominated by one relevant model-independent near-threshold pole which, for $E_B = 0.5$ MeV and $\Lambda = 500$ MeV, is still located at $k_1 = i31.1$ MeV equal to the value of k_1 for the single-channel case given in Eq. (66). The position of other poles is very model-dependent, however they all are in general located quite far away from the threshold.

Following the same lines as in the single-channel case above, one can find the residue of the amplitude a_{00} at $E = -E_B$. The dependence of the residue squared on the binding energy for $\Lambda = 500$ MeV is illustrated in Fig. 3 by the lower (blue) dotted line. To a good approximation, the dependence of the residue on the binding energy can be written as

$$\text{Res } a_{00} \approx \frac{\text{const}(\Lambda)}{\pi\mu_{0*}^2} \frac{\kappa_c(E_B)\kappa_0(E_B)}{\kappa_c(E_B) + \kappa_0(E_B)} \left(1 - \frac{8}{\pi\Lambda}\frac{\kappa_c(E_B)\kappa_0(E_B)}{\kappa_c(E_B) + \kappa_0(E_B)}\right)^{-1}, \tag{76}$$

where $\kappa_c(E_B) = \sqrt{2\mu_{c*}(E_B + \Delta M)}$, $\kappa_0(E_B) = \sqrt{2\mu_{0*}E_B}$, and const$(\Lambda)$ is a constant of order of unity. In the limit of small binding energies $(E_B \ll \Delta M)$, one has $\kappa_0(E_B) \ll \kappa_c(E_B)$, and the formula for the residue (76) can be simplified as

$$\text{Res } a_{00} \approx \text{const} \cdot \frac{\kappa_0(E_B)}{\pi\mu_{0*}^2}\left(1 - \frac{8}{\pi\Lambda}\kappa_0(E_B)\right)^{-1}, \tag{77}$$

so that, similarly to the single-channel case [compare with Eq. (69)], the residue squared remains approximately linear with E_B, up to small finite-range corrections. In principle, the

range of validity of this expression is rather limited since the correction $\sim \sqrt{E_B}$ from $\kappa_c(E_B)$ starts to play a role quite rapidly. However, an analogous correction but with an opposite sign appears also from the finite-range term ($\sim 1/\Lambda$) in the denominator. This leads to a partial cancellation of these terms.

Interestingly, for $E_B \sim \Delta M$, the linear behaviour of the residue squared as a function of E_B is still approximately preserved since again the finite-range corrections are cancelled to a large extent by the corrections due to $\kappa_c(E_B)$. As a result, for $\Lambda =500$ MeV, the behaviour of the residue squared is almost exactly linear in the whole range of E_B. This linearity is, of course, accidental—for larger cut offs the deviation from the straight line is more pronounced; however, it remains a correction to the leading linear behaviour.

Deviations from the Weinberg prediction are expected to be of order $r\sqrt{2\mu_{0*}E_B}$, with r being the range of forces. If we estimate the latter by r_{eff} from above, $r_{\mathrm{eff}}\sqrt{2\mu_{0*}E_B} \sim 0.1\sqrt{E_B/\mathrm{MeV}}$, we expect a deviation of the residue from the Weinberg prediction of the order of 30% at $E_B = 7$ MeV, in line with what can be read off from Fig. 3 for the single-channel curve. As explained above, accidental cancellations make the result for the coupled-channel calculation more consistent with a linear behaviour than expected naively.

The influence of the coupled-channel dynamics on the residue can be better understood if one considers the limit $\Lambda \to \infty$. In this case, as follows from Eqs. (69) and (76), the ratio of the residue for the coupled-channel problem to that for the single-channel one reads

$$R = \frac{\mathrm{Res}\, a_{00}(\text{coupled-channel})}{\mathrm{Res}\, a_{00}(\text{single-channel})} \underset{\Lambda \to \infty}{=} \left(1 + \sqrt{\frac{E_B}{E_B + \Delta M}}\right)^{-1}, \qquad (78)$$

where we neglected the tiny difference between μ_{0*} and μ_{c*} and used the fact that $\mathrm{const}(\Lambda) \to 1$ when $\Lambda \to \infty$. It is clear from the ratio (78) that the coupled-channel effect is negligible at small binding energies, $E_B \ll \Delta M$, that is, once we stay close to one threshold, its effect dominates over the effect of the other, remote, threshold. In the opposite limit, for $E_B \gg \Delta M$, when the splitting between thresholds can be neglected, this ratio tends to one half, that is, in agreement with natural expectations, asymptotically both thresholds contribute equally to the residue.

3. Counter-term in presence of dynamical pions

The behaviour of the counter term C_0 versus Λ in the full single-channel problem ($D^0 \bar{D}^{0*}$) with dynamical pions is shown in the left panel of Fig. 4 by the blue dotted curve. The figure demonstrates a clear limit-cycle behaviour of the contact term with the increase of Λ in full analogy with the NN [35] and 3N [36] problems, see also Refs. [37–39] for related works. Meanwhile, a plateau between the first negative and positive infinite solutions is about 7 GeV for the $D\bar{D}^*$ problem which is much larger than that for NN [35].

The behaviour of the counter term C_0 on the cut off Λ in the two-channel case, when dynamical pions are present in the problem, is illustrated in the right panel of Fig. 4. We therefore solve the full problem—see Sec. II C. In contradistinction to the one-channel case (and to the NN case), in a coupled-channel problem there are two solutions for $C_0(\Lambda)$ that correspond to a resonance with the peak at $E_B = 0.5$ MeV [see the quadratic equation (75) and the discussion in the previous section]. These solutions, shown as solid red and dashed black curves in the right panel of Fig. 4, again exhibit a sort of limit-cycle behaviour individually. However, it is interesting to observe that there are regions of cut offs where no solution for $C_0(\Lambda)$ exists. This can be understood as follows: for values of Λ, where the two solutions for $C_0(\Lambda)$ approach each other (see, for example, the region of Λ just above 2 GeV), a second singularity approaches the $D\bar{D}^*$ threshold. As a consequence, the two approaching states start to repel each other to avoid a crossing of the levels. Therefore there is a region of E_B where the peak of the resonance cannot be reached by any variation of the strength of the potential $C_0(\Lambda)$. The regions of Λ corresponding to the absence of the resonance peak at $E_B = 0.5$ MeV for any values of $C_0(\Lambda)$ are illustrated in the right panel of Fig. 4. Further details on the limit cycle behaviour in many-channel problems will be provided in a subsequent publication.

What should be stressed here is that as long as we choose the cut off to be relatively far away from the problematic region one of the states is always located far away from the threshold and therefore should not affect observables. As a consequence, observables are basically independent of whether one or the other branch of C_0 is chosen—see Sec. III B.

A comment is in order here concerning the role played by the OPE for the binding of the X meson. From Fig. 4 one can see that for particular values of the cut off (for example, for
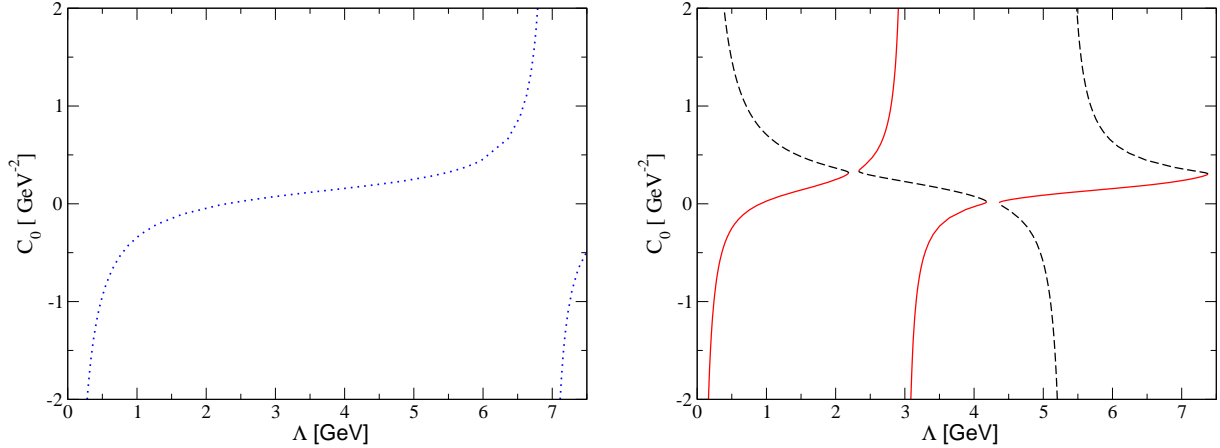
FIG. 4: Left panel: Behaviour of the counter term C_0 versus Λ in the full single-channel problem $(D^0 \bar{D}^{0*})$ with dynamical pions. Right panel: Behaviour of C_0 as a function of the cut off Λ in the full two-channel problem with dynamical pions.

$\Lambda \approx 900$ MeV in the coupled-channel problem), there is a solution with $C_0 = 0$ which could be naively taken for the bound state in the pure OPE potential with dynamical pions. This is not the case however since the details of the short-ranged dynamics are simply hidden in the particular cut off pattern for the divergent integrals taking place for such Λ's. Furthermore, in previous chapters, we showed how to arrive at the bound state with a purely contact potential. Finally, the bound state can be found in a combined short-range+OPE potential with C_0 varying from $-\infty$ to ∞, as shown in Fig. 4. Since physical observables, for example, the width of the X-meson (see below) are almost Λ-independent in a large interval of Λ's, then no model-independent statement is possible concerning the importance of the one-pion exchange for the formation of the $X(3872)$, contrary to earlier claims [16, 19].

B. The effect of dynamical pions on a near-threshold resonance

With the experience gained in the previous chapter, we are in a position to perform a detailed numerical analysis of the system (48). We compare the following three situations:

1. The single-channel problem in the static approximation, that is we solve the system (48) with $V_{c0}^{mn}(\boldsymbol{p}, \boldsymbol{p}') = V_{0c}^{mn}(\boldsymbol{p}, \boldsymbol{p}') = V_{cc}^{mn}(\boldsymbol{p}, \boldsymbol{p}') = 0$ and with the static OPE potential which, as before, is given by Eq. (39), but with $\alpha_{00} = \alpha'_{00} = 1$ and with

$$D_{300}^{\text{static}}(\boldsymbol{p}, \boldsymbol{p}') = 2m_0 + m_{\pi^0} + \frac{(\boldsymbol{p} + \boldsymbol{p}')^2}{2m_{\pi^0}} - (m_{0*} + m_0) - i0 \tag{79}$$

for the inverse three-body propagator. In addition, instead of the running width (52), we use a constant width

$$\Gamma_0 = 63 \text{ keV.} \tag{80}$$

Note that in the absence of the three-body dynamics both these effects, the constant width and the imaginary part of the potential, represent the same effect of the decay $D^* \to D\pi$ related to two-body unitarity. Thus, keeping only one of these effects would lead to inconsistent treatment.

2. The full dynamical calculation for the single-channel problem, including the three-body $\pi D\bar{D}$ intermediate states as well as the dynamical width of the D^*. For the D^{*0} width we use formula (52) without the contribution of the charged channels.

3. The full dynamical calculation of the two-channel problem, including three-body $D\bar{D}\pi$ intermediate states as well as the dynamical width of the D^*, as was explained in Sec. II C.

First, we investigate the effect of dynamical pions on the residue of the scattering amplitude a_{00} squared—see Fig. 3 and the discussion in Sec. III A. The upper (red) and lower (blue) solid curves correspond to case 2 and case 3 above, respectively. As was discussed before, the solid curves lie on top of the dotted curves indicating that the binding energy dependence of the residue is basically independent of the dynamics. The closeness of the results to the straight line (black dot-dashed curve in Fig. 3) indicates the dominance of the single-pole scenario and thus the molecular nature of the $X(3872)$ meson.

In Fig. 5 we show the results for the production rate dBr/dE corresponding to all three different cases described above: (i) solution of the single-channel problem in the static limit— (green) dot–dashed line; (ii) solution of the single-channel dynamical calculation—(blue) dashed line; (iii) solution of the full two-channel dynamical problem—(red) solid line. In all cases the value of the cut off Λ was fixed to 500 MeV and the strength of the contact operator C_0 was adjusted such that the $D^0\bar{D}^{*0}$ scattering amplitude has a resonance state peaked at $E = -E_B = -0.5$ MeV. All curves are normalised to obey the same energy behaviour near the three-body $D^0\bar{D}^0\pi^0$ threshold, located at $E = -7.15$ MeV. The difference between them is visible only in the region of the peak and is pronounced in the different strength of
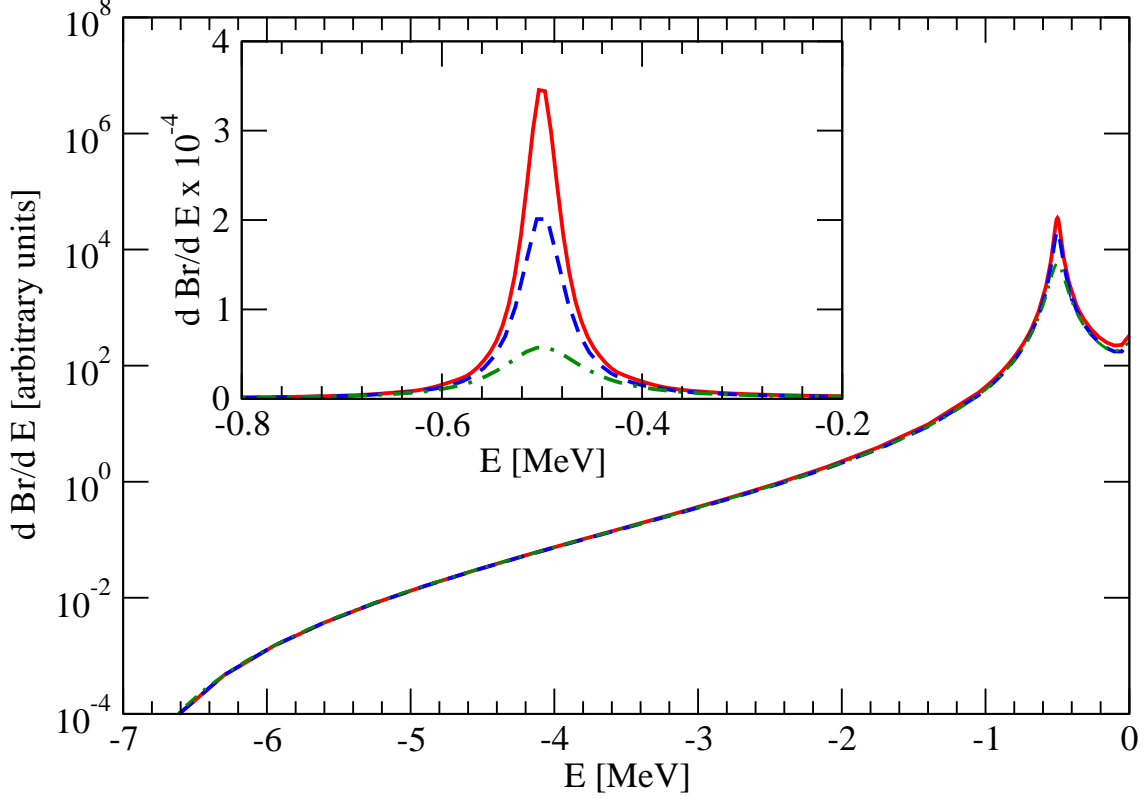
FIG. 5: Production rate (in logarithmic scale) for the three calculations as described in the text: (i) solution of the single-channel problem in the static limit—(green) dot-dashed line; (ii) solution of the single-channel dynamical calculation—(blue) dashed line; (iii) solution of the full two-channel dynamical problem—(red) solid line. All curves are normalised near the $D^0 \bar{D}^0 \pi^0$ threshold, located at $E = -7$ MeV. The inlay shows a zoom into the peak region in linear scale.

the peaks—see Fig. 5. If one normalises all three curves at the peak, the difference in the resonance region shows up only in the different widths of the resonance. To quantify the effect we notice that, in the energy region around the resonance peak, the $D\bar{D}^*$ scattering amplitude a_{00} acquires basically a separable form:

$$a_{00}^{SS}(\boldsymbol{p}, \boldsymbol{p}', E) = -\frac{1}{\mu_{0*}\pi} f(E)\phi(\boldsymbol{p})\phi(\boldsymbol{p}'), \tag{81}$$

with ϕ being a formfactor, so that the energy-dependent amplitude $f(E)$ is factored out from the integration over the phase space in Eq. (54). Parametrising $f(E)$ by the Breit–Wigner (BW) shape, one finds for the rate:

$$\left(\frac{dBr}{dE}\right)_{\text{BW}} = \frac{\text{const}}{(E + E_B)^2 + \Gamma_X^2/4} \, \hat{k}_{\text{eff}}(E), \tag{82}$$

where $\hat{k}_{\text{eff}}(E)$ corresponds to the integral over the phase space in Eq. (54) with $J(p, E) = 1$. Except for the region very close to the threshold, $\hat{k}_{\text{eff}}(E)$ is a very smooth function of energy around the peak as compared to the Breit–Wigner shape. Therefore, expression (82) can be used to extract the width Γ_X. The results for Γ_X extracted for all three cases above are shown in Table I. Examining the transition from case 2 to case 3, one can see that including the charge channel changes the shape of the spectrum only marginally. The nearest threshold which affects the observables due to the coupled-channel effect is $D^+\bar{D}^0\pi^-$ (and $D^-D^0\pi^+$) which is about 2.5 MeV above the $D^0\bar{D}^{*0}$ threshold. Also the $D^+D^-\pi^0$ threshold is just 3 MeV above the $D^0\bar{D}^{*0}$ threshold. Had the mass of the charged D-meson been smaller by $2.5 - 3$ MeV and more, the new cuts would have occurred in the $D\bar{D}^*$ potential increasing the $X(3872)$ width and thus emphasising the role of the coupled-channel dynamics. In the meantime, the transition from case 1 to case 2 elucidates the role of the three-body dynamics: switching on three-body effects makes the resonance narrower by a factor of 2.

In order to quantify the role of the pion dynamics in the vicinity of the threshold we use the scattering length approximation and study the impact of the three-body dynamics on the $D^0\bar{D}^{*0}$ scattering length. The molecule scenario for the $X(3872)$ implies that, near threshold, the effective-range corrections are small (which is also in agreement with the nearly linear behaviour of the residue as a function of the binding energy in Fig. 3), so we resort to the scattering length (SL) approximation for the production rate:

$$\left(\frac{dBr}{dE}\right)_{\text{SL}} = \text{const} \times |f(E)|^2 \, \hat{k}_{\text{eff}}(E), \quad f(E) = \frac{1}{-\gamma_1 - i\gamma_2 - i\sqrt{2\mu_{0*}(E + i0)}}. \tag{83}$$

A similar approach to the analysis of the $DD\pi$ line shape was used in Ref. [25], where the width of the X originated from a constant D^{0*} width in the absence of inelastic channels. In Eq. (83) we also neglect inelastic effects from remote thresholds and introduce γ_2 to account for the change of the X width due to the $D\bar{D}\pi$ intermediate states in the energy region near the $D\bar{D}^*$ threshold. Stated differently, γ_2 accounts for the shift of the pole position in the complex plane due to the three-body dynamics. Parameters γ_1 and γ_2 ($\gamma_2 > 0$ from unitarity) corresponding to the full dynamical treatment can be well determined from a fit to the resonance structure in the line shape—see Fig. 5.

Case	E_B, MeV	Γ_X, keV	γ_1, MeV	γ_2, MeV
Case 1	0.5	102	31.1	1.58
Case 2	0.5	53	31.1	0.82
Case 3	0.5	44	31.1	0.68

TABLE I: Parameters of the distributions (82) and (83) extracted from the fit to the peak for the line shapes depicted in Fig. 5.

Near the peak, that is for $|E + E_B| \ll E_B$, the scattering length formula (83) is identical to the Breit–Wigner one (82) with the following identification of the parameters:

$$E_B = \frac{\gamma_1^2 - \gamma_2^2}{2\mu_{0*}}, \quad \Gamma_X = \frac{2\gamma_1\gamma_2}{\mu_{0*}}. \tag{84}$$

Furthermore, for a narrow resonance ($\Gamma_X \ll E_B$), these relations can be inverted to give:

$$\gamma_1 \approx \sqrt{2\mu_{0*}E_B}, \quad \gamma_2 \approx \frac{\mu_{0*}\Gamma_X}{\sqrt{2\mu_{0*}E_B}}. \tag{85}$$

Clearly, a reduction of the X width by a factor of 2 would necessarily suppress γ_2 by the same amount. The results for γ_1 and γ_2 for three different scenarios from above are quoted in Table I. It should be noted that the expression (83) provides a very good approximation for the exact line shape in the near-threshold region even relatively far away from the pole, for $|E + E_B| \sim E_B$.

We would like to stress also that the effect of pion dynamics depends strongly on the position of the resonance state relative to the relevant two- and three-body thresholds. Indeed, once it approaches the three-body $D^0\bar{D}^0\pi^0$ threshold, the imaginary parts originating from the three-body effects vanish, and the X width tends to a constant due to the $D^{0*} \to D^0\gamma$ transition, while the X width in the static approximation stays nearly constant—see left panel of Fig. 6. On the other hand, the dynamical width of the $X(3872)$ grows as the resonance peak approaches the two-body $D^0\bar{D}^{*0}$ threshold. The dependence of the effective X width Γ_X [as well as that of the γ_2 by virtue of Eq. (85)] on the binding energy can be parametrised in the interval from 0.1 to 2 MeV in an analytic form:

$$\Gamma_X(E_B) = \frac{\Gamma_1\beta_1^2}{E_B^2 + \beta_1^2} + \frac{\Gamma_2\beta_2^2}{E_B^2 + \beta_2^2}, \tag{86}$$
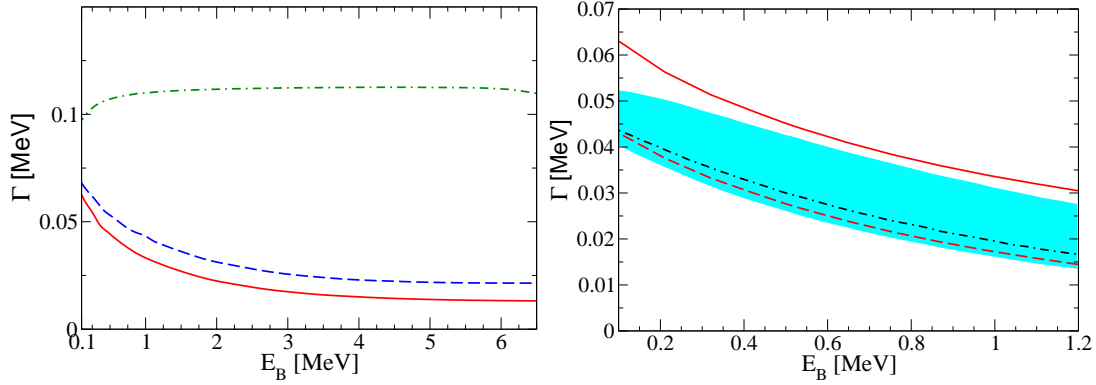
FIG. 6: The X width as a function of the binding energy E_B. Left panel: The results of three calculations as explained in the text; the notation of curves is as in Fig. 5. Right panel: Comparison of our results [red solid (dashed) curve including (omitting) the $\bar{D}^*D\gamma$ width] with those of Refs. [21, 30] (dot–dashed line for the LO calculation of Ref. [30] and blue band for the NLO calculation of Ref. [21], respectively).

with $\Gamma_1 = 35.5$ keV, $\beta_1 = 2.369$ MeV, $\Gamma_2 = 28.7$ keV, and $\beta_2 = 0.364$ MeV. In this form the effect of dynamical pions can be conveniently incorporated in the analysis of experimental data.

In the right panel of Fig. 6 the results of our full dynamical calculation are confronted with those of the X-EFT [21, 30]. In leading order (LO) of X-EFT [30] pion degrees of freedom are integrated out, and the wave function of the X, as a bound state, is taken in a universal form provided by the contact $D\bar{D}^*$ interaction. Then the X width is calculated as an integral over the three-body phase space from the product of the X wave function and the decay vertex $D^{*0} \to D^0\pi^0$. The result of Ref. [30] is improved in Ref. [21] by taking next-to-leading (NLO) corrections. The counting scheme used in Ref. [21] treats the pion effects perturbatively in distinction from the nonperturbative inclusion of the LO contact operators in analogy to what was proposed for the NN system in Refs. [40]. The results of these two calculations (taken from Fig. 7 of Ref. [21]) are shown in the right panel of Fig. 6 by the dot-dashed curve (LO) and by the blue band (NLO), respectively. For the

sake of comparison our result[1] is given in the right panel of Fig. 6 as the (red) solid and dashed lines, where the former is the result for the full calculation, while the latter is the result when the $D\bar{D}\gamma$ channel is omitted—since this contribution to the width was not included in the X-EFT calculations, it is this curve that is to be compared to the results of Refs. [21, 30]. We are therefore to conclude that the X-EFT reproduces the results of our more complete calculation very nicely. This level of agreement provides strong support of the power counting underlying the X-EFT.

All the results shown in Figs. 5 and 6 were calculated with $\Lambda = 500$ MeV, and the value of C_0 for the full problem (case 3) was chosen to be negative, see solid (red) branch in the right panel of Fig. 4. Note, however, that the variation of the results with the cutoff is very mild for the range of Λ from 300 to 1700 MeV and from 2500 to 3800 MeV. For example, varying Λ in the range 300 MeV $\lesssim \Lambda \lesssim$ 1700 MeV influences the width only at a few percent level comparable with the numerical noise. Also we obtain that choosing another branch of C_0 results in the uncertainty in the width of a similar (small) size.

As the final remark let us mention that, aiming at the effects related to dynamical pions, we considered only the part of the $X(3872)$ width that comes from the $D\bar{D}\pi$ intermediate state. The physical $X(3872)$ supposedly acquires a significant part of its width from inelastic channels like $J/\psi\pi\pi$ and $J/\psi\pi\pi\pi$. However, the effects discussed here should be of relevance for the line shapes of the $X(3872)$ in the $D\bar{D}\pi$ channel.

IV. SUMMARY

We investigated the role played by dynamical pions on the structure of the $X(3872)$ by solving the full three-body $D\bar{D}\pi$ problem. The two-body $\pi D \to \pi D$ input is fixed by the width of the D^*, however, a short-ranged $D\bar{D}^* \to D\bar{D}^*$ contact term needed to be introduced to arrive at well defined equations. Depending on the regulator used for solving the equations, the contact term can take values between $-\infty$ and $+\infty$ for the cut

---

[1]We would like to stress that in both above-mentioned calculations the X is assumed to be a genuine bound (not a resonance) state. In the full treatment, however, such a bound state does not exist, so that one cannot calculate the width directly, following the lines of Refs. [21, 30]. Instead, one is left to extract the X width using the procedure described above in this chapter.

off regularisation scheme. On the other hand, the strength of the one-pion exchange is fixed. Thus, the relative importance of the pion exchange as compared to the short-ranged contributions to the $D\bar{D}^*$ scattering potential appears to be strongly regulator-dependent. We are therefore led to conclude that no model independent statement on the importance of the one-pion exchange for the formation of the $X(3872)$ is possible, contrary to earlier claims [16, 19].

In addition, we found that the residue for $X \to D\bar{D}^*$ is weakly dependent on the kind of pion dynamics included. Especially, the dependence of the residue on the X binding energy is very close for a fully dynamical calculation and for a calculation with a contact-type interaction only. A deviation between the coupled-channel and the single-channel treatment is clearly observed but with the larger effect for binding energies beyond 1 MeV.

The most striking effect of dynamical pions is observed in their impact on the X line shapes: in the fully dynamical calculation the width from the $D\bar{D}\pi$ intermediate states appears to be reduced by about a factor of 2, from 102 down to 44 keV, assuming that the $X(3872)$ corresponds to a resonance state with a peak at 0.5 MeV below the $D\bar{D}^*$ threshold. Stated differently, by using the naive static approximation for the $D\bar{D}\pi$ intermediate states one overestimates substantially their effect on the X width. Although the total width of the X is rather saturated by inelastic channels like $J/\psi\pi\pi$ and $J/\psi\pi\pi\pi$, our findings should be of relevance for the predicted line shape in the $D^0\bar{D}^0\pi^0$ channel, where the signal below the $D\bar{D}^*$ threshold is controlled exactly by the $D\bar{D}\pi$ cuts. For example, if the line shape near threshold is analysed within the scattering length approximation, the imaginary part of the inversed scattering length, γ_2, which is the only parameter affected by the three-body dynamics, has to be taken from the fully dynamical calculation. The parameter γ_2 (and thus the role of pion dynamics) appears to be a smooth but vivid function of the binding energy, for which we provide a simple analytic parameterisation suitable to mimic three-body effects numerically in the data analysis.

On the contrary, the effect of the coupled-channel dynamics on the X width turned out to be rather moderate, which can be attributed to the fact that both the real part of the resonance pole E_B and the X width Γ_X are small as compared to the separation ΔM between the neutral and the charged thresholds.

Our results for the X width and for the residue appear to be in good agreement with those obtained in the X-EFT approach [21, 30], which justifies the central assumption underlying

the X-EFT that pions can be treated perturbatively. In addition, an important progress achieved in our work due to considering the full coupled-channel dynamics with nonperturbative pions is that pion range corrections are included to all orders in our calculation. Because of the proximity of the $D\bar{D}\pi$ threshold, those are expected to give a prominent contribution to the range corrections even beyond leading order. We therefore expect the nonperturbative calculation to have a smaller uncertainty than that with the perturbative treatment of pions. In addition, the X pole is located very close to both the $D\bar{D}\pi$ as well as the $D\bar{D}^*$ thresholds, which all influence the pertinent integrals. Thus, although for the X the effects can be nicely absorbed into a counter term, this is not necessarily the case anymore for other, related resonances, say in the B sector[2]. In this sense our calculation appears as an important step for a common understanding of a larger class of quarkonium resonances.

Acknowledgments

---

[1] N. Brambilla, *et al.*, Eur. Phys. J. C **71**, 1534 (2011).

[2] S. K. Choi *et al.* [Belle Collaboration], Phys. Rev. Lett. **91**, 262001 (2003).

[3] A. Abulencia *et al.* [CDF Collaboration], Phys. Rev. Lett. **98**, 132002 (2007).

[4] P. del Amo Sanches *et al.* [BABAR Collaboration], Phys. Rev. D **82**, 011101 (2010).

[5] M. Suzuki, Phys. Rev. D **72**, 114013 (2005).

[6] D. Gamermann and E. Oset, Phys. Rev. D **80**, 014003 (2009).

[7] G. Gokhroo *et al.* [Belle Collaboration], Phys. Rev. Lett. **97**, 162002 (2006).

---

[2] A first step towards a combined study of $D^{(*)}\bar{D}^{(*)}$ and $B^{(*)}\bar{B}^{(*)}$ was taken in Ref. [41].

[8] B. Aubert *et al.* [BaBar Collaboration], Phys. Rev. D **77**, 011102 (2008).

[9] T. Aushev *et al.* [Belle Collaboration], Phys. Rev. D **81**, 031103 (2010).

[10] Yu. S. Kalashnikova and A. V. Nefediev, Phys. Rev. D **82**, 097502 (2010).

[11] Yu. S. Kalashnikova, Phys. Rev. D **72**, 034010 (2005).

[12] I. V. Danilkin and Yu. A. Simonov, Phys. Rev. Lett. **105**, 102002 (2010).

[13] P. Artoisenet, E. Braaten, and D. Kang, Phys. Rev. D **82**, 014013 (2010).

[14] M. B. Voloshin and L. B. Okun, Pisma Zh. Eksp. Teor. Fiz. **23**, 369 (1976) [JETP Lett. **23**, 333 (1976)].

[15] N. A. Tornqvist, Phys. Rev. Lett. **67**, 556 (1991).

[16] N. A. Tornqvist, Phys. Lett. B **590**, 209 (2004).

[17] E. S. Swanson, Phys. Lett. B **588**, 189 (2004).

[18] Yan-Rui Liu, Xiang Liu, Wei-Zhen Deng, and Shi-Lin Zhu, Eur. Phys. J. C **56**, 63 (2008).

[19] C. E. Thomas and F. E. Close, Phys. Rev. D **78**, 034007 (2008).

[20] E. Braaten, M. Lu, and J. Lee, Phys. Rev. D **76**, 054010 (2007).

[21] S. Fleming, M. Kusunoki, T. Mehen, and U. van Kolck, Phys. Rev. D **76**, 034006 (2007).

[22] A. Filin *et al*, Phys. Rev. Lett. **105**, 019101 (2010).

[23] F. E. Close and C. Downum, Phys. Rev. Lett. **102**, 242003 (2009); F. E. Close, C. Downum, and C. E. Thomas, Phys. Rev. D **81**, 074033 (2010).

[24] E. Braaten and M. Lu, Phys. Rev. D **76**, 094028 (2007);

[25] E. Braaten and J. Stapleton, Phys. Rev. D **81**, 014019 (2010).

[26] C. Hanhart, Yu. S. Kalashnikova, and A. V. Nefediev, Phys. Rev. D **81**, 094028 (2010).

[27] Yu. S. Kalashnikova and A. V. Nefediev, Phys. Rev. D **80**, 074004 (2009); Yu. S. Kalashnikova, A. E. Kudryavtsev, and A. V. Nefediev, Phys. At. Nucl. **73**, 1592 (2010).

[28] P. Hagen, H.-W. Hammer, and C. Hanhart, Phys. Lett. B **696**, 103 (2011).

[29] T. Mehen and R. Springer, Phys. Rev. D **83**, 094009 (2011); E. Braaten, H.-W. Hammer, and T. Mehen, Phys. Rev. D **82**, 034018 (2010); S. Fleming, T. Mehen, Phys. Rev. D **78**, 094019 (2008).

[30] M. B. Voloshin, Phys. Lett. B **579**, 316 (2004).

[31] R. Aaron, R. D. Amado, and J. E. Young, Phys. Rev. **174**, 2022 (1968).

[32] S. Weinberg, Phys. Rev. **130**, 776 (1963); *ibid* **131**, 440 (1963); *ibid* **137**, B672 (1965).

[33] V. Baru *et al.*, Phys. Lett. B **586**, 53 (2004).

[34] D. Morgan, Nucl. Phys. A **543**, 632 (1992).

[35] A. Nogga, R. G. E. Timmermans, and U. van Kolck, Phys. Rev. C **72**, 054006 (2005).

[36] P. F. Bedaque, H. W. Hammer, and U. van Kolck, Phys. Rev. Lett. **82**, 463 (1999); Nucl. Phys. A **676**, 357 (2000).

[37] A. E. Kudryavtsev, V. E. Markushin, and I. S. Shapiro, Zh. Eksp. Teor. Fiz. **74**, 432 (1978); A. E. Kudryavtsev and V. S. Popov, Pisma Zh. Eksp. Teor. Fiz. **29**, 311 (1979).

[38] S. R. Beane, P. F. Bedaque, M. J. Savage, and U. van Kolck, Nucl. Phys. A **700**, 377 (2002).

[39] E. Braaten and D. Phillips, Phys. Rev. A **70**, 052111 (2004).

[40] D. B. Kaplan, M. J. Savage, and M. B. Wise, Phys. Lett. B **424**, 390 (1998); Nucl. Phys. B **534**, 329 (1998).

[41] J. Nieves and M. P. Valderrama, Phys. Rev. D **84**, 056015 (2011).

Appendix A: Details of the derivation of the three–body equation (26)

After excluding the third equation, the systems (17) and (18), with all arguments and sub(super)scripts restored, read

$$
\begin{cases}
t_{22}^{mn}(\boldsymbol{p}, \boldsymbol{p}', E) = -\Sigma(p)\delta^{mn}\delta(\boldsymbol{p} - \boldsymbol{p}') + \dfrac{\Sigma(p)}{D_2(\boldsymbol{p})}t_{22}^{mn}(\boldsymbol{p}, \boldsymbol{p}', E) \\
\qquad\qquad + g^2 \displaystyle\int d^3q \dfrac{q_m(\alpha q_p + \beta p_p)}{D_3(\boldsymbol{p}, \boldsymbol{q})D_2(-\boldsymbol{q} - \alpha\boldsymbol{p})}t_{\bar{2}2}^{pn}(-\boldsymbol{q} - \alpha\boldsymbol{p}, \boldsymbol{p}', E) \\[1.2em]
t_{\bar{2}2}^{mn}(\boldsymbol{p}, \boldsymbol{p}', E) = -g^2 \dfrac{(\alpha p_m + p'_m)(\alpha p'_n + p_n)}{D_3(\boldsymbol{p}, -\alpha\boldsymbol{p} - \boldsymbol{p}')} + \dfrac{\Sigma(p)}{D_2(\boldsymbol{p})}t_{\bar{2}2}^{mn}(\boldsymbol{p}, \boldsymbol{p}', E) \\
\qquad\qquad + g^2 \displaystyle\int d^3q \dfrac{q_m(\alpha q_p + \beta p_p)}{D_3(\boldsymbol{p}, \boldsymbol{q})D_2(-\boldsymbol{q} - \alpha\boldsymbol{p})}t_{22}^{pn}(-\boldsymbol{q} - \alpha\boldsymbol{p}, \boldsymbol{p}', E),
\end{cases} \tag{A1}
$$

$$
\begin{cases}
t_{\bar{2}\bar{2}}^{mn}(\bar{\boldsymbol{p}}, \bar{\boldsymbol{p}}', E) = -\Sigma(\bar{p})\delta^{mn}\delta(\bar{\boldsymbol{p}} - \bar{\boldsymbol{p}}') + \dfrac{\Sigma(\bar{p})}{D_2(\bar{\boldsymbol{p}})}t_{\bar{2}\bar{2}}^{mn}(\bar{\boldsymbol{p}}, \bar{\boldsymbol{p}}', E) \\
\qquad\qquad + g^2 \displaystyle\int d^3\bar{q} \dfrac{\bar{q}_m(\alpha \bar{q}_p + \beta \bar{p}_p)}{D_3(\bar{\boldsymbol{p}}, \bar{\boldsymbol{q}})D_2(-\bar{\boldsymbol{q}} - \alpha\bar{\boldsymbol{p}})}t_{2\bar{2}}^{pn}(-\bar{\boldsymbol{q}} - \alpha\bar{\boldsymbol{p}}, \bar{\boldsymbol{p}}', E) \\[1.2em]
t_{2\bar{2}}^{mn}(\bar{\boldsymbol{p}}, \bar{\boldsymbol{p}}', E) = -g^2 \dfrac{(\alpha \bar{p}_m + \bar{p}'_m)(\alpha \bar{p}'_n + \bar{p}_n)}{D_3(\bar{\boldsymbol{p}}, -\alpha\bar{\boldsymbol{p}} - \bar{\boldsymbol{p}}')} + \dfrac{\Sigma(\bar{p})}{D_2(\bar{\boldsymbol{p}})}t_{2\bar{2}}^{mn}(\bar{\boldsymbol{p}}, \bar{\boldsymbol{p}}', E) \\
\qquad\qquad + g^2 \displaystyle\int d^3\bar{q} \dfrac{\bar{q}_m(\alpha \bar{q}_p + \beta \bar{p}_p)}{D_3(\bar{\boldsymbol{p}}, \bar{\boldsymbol{q}})D_2(-\bar{\boldsymbol{q}} - \alpha\bar{\boldsymbol{p}})}t_{\bar{2}\bar{2}}^{pn}(-\bar{\boldsymbol{q}} - \alpha\bar{\boldsymbol{p}}, \bar{\boldsymbol{p}}', E).
\end{cases} \tag{A2}
$$

It can be demonstrated then that $t_{23}^m(\boldsymbol{p}; \boldsymbol{p}', \boldsymbol{q}')$ and $t_{\bar{2}3}^m(\bar{\boldsymbol{p}}; \bar{\boldsymbol{p}}', \bar{\boldsymbol{q}}')$ of the form

$$
t_{23}^m(\boldsymbol{p}; \boldsymbol{p}', \boldsymbol{q}'; E) = g q'_m \delta(\boldsymbol{p} - \boldsymbol{p}') - \dfrac{g}{D_2(\boldsymbol{p}')}t_{22}^{mn}(\boldsymbol{p}, \boldsymbol{p}', E)q'_n
$$

$$- \frac{g}{D_2(-\boldsymbol{q}' - \alpha\boldsymbol{p}')} t_{22}^{mn}(\boldsymbol{p}, -\boldsymbol{q}' - \alpha\boldsymbol{p}', E)(\alpha q_n' + \beta p_n'), \tag{A3}$$

$$t_{23}^m(\bar{\boldsymbol{p}}; \bar{\boldsymbol{p}}', \bar{\boldsymbol{q}}'; E) = g\bar{q}_m'\delta(\bar{\boldsymbol{p}} - \bar{\boldsymbol{p}}') - \frac{g}{D_2(\bar{\boldsymbol{p}}')} t_{22}^{mn}(\bar{\boldsymbol{p}}, \bar{\boldsymbol{p}}', E)\bar{q}_n'$$

$$- \frac{g}{D_2(-\bar{\boldsymbol{q}}' - \alpha\bar{\boldsymbol{p}}')} t_{22}^{mn}(\bar{\boldsymbol{p}}, -\bar{\boldsymbol{q}}' - \alpha\bar{\boldsymbol{p}}', E)(\alpha\bar{q}_n' + \beta\bar{p}_n'). \tag{A4}$$

satisfy the last system, given by Eq. (19).

Equations for the C-even and C-odd $D\bar{D}^*$ matrix elements

$$t_\pm = t_{22} \pm t_{\bar{2}2}, \tag{A5}$$

take the form:

$$t_\pm^{mn}(\boldsymbol{p}, \boldsymbol{p}', E) = -\frac{\Sigma(p)D_2(\boldsymbol{p})}{\Delta(p)}\delta^{mn}\delta(\boldsymbol{p} - \boldsymbol{p}') \mp g^2\frac{(\alpha p_m + p_m')(\alpha p_n' + p_n)}{D_3(\boldsymbol{p}, -\alpha\boldsymbol{p} - \boldsymbol{p}')}\frac{D_2(\boldsymbol{p})}{\Delta(p)}$$

$$\pm g^2\frac{D_2(\boldsymbol{p})}{\Delta(p)} \int d^3s \frac{(s_m + \alpha p_m)(\alpha s_p + p_p)}{D_3(\boldsymbol{p}, -\boldsymbol{s} - \alpha\boldsymbol{p})D_2(\boldsymbol{s})} t_\pm^{pn}(\boldsymbol{s}, \boldsymbol{p}', E), \tag{A6}$$

which can be brought to the form of Eq. (26) by the substitution

$$t_\pm^{mn}(\boldsymbol{p}, \boldsymbol{p}', E) = -\frac{\Sigma(p)D_2(\boldsymbol{p})}{\Delta(p)}\delta^{mn}\delta(\boldsymbol{p} - \boldsymbol{p}') + \frac{D_2(\boldsymbol{p})}{\Delta(p)}a_\pm^{mn}(\boldsymbol{p}, \boldsymbol{p}', E)\frac{D_2(\boldsymbol{p}')}{\Delta(p')}. \tag{A7}$$